ACS central science

Research Article

Pairing *Bacteroides vulgatus* LPS Structure with Its Immunomodulatory Effects on Human Cellular Models

Flaviana Di Lorenzo,* Molly D. Pither, Michela Martufi, Ilaria Scarinci, Joan Guzmán-Caldentey, Ewelina Łakomiec, Wojciech Jachymek, Sven C. M. Bruijns, Sonsoles Martín Santamaría, Julia-Stephanie Frick, Yvette van Kooyk, Fabrizio Chiodo, Alba Silipo, Maria Lina Bernardini, and Antonio Molinaro*

Cite This: *ACS Cent. Sci.* 2020, 6, 1602−1616

Read Online

ACCESS | Metrics & More | Article Recommendations | Supporting Information

ABSTRACT: The gut microbiota guide the development of the host immune system by setting a systemic threshold for immune activation. Lipopolysaccharides (LPSs) from gut bacteria are able to trigger systemic and local proinflammatory and immunomodulatory responses, and this capability strongly relies on their fine structures. Up to now, only a few LPS structures from gut commensals have been elucidated; therefore, the molecular motifs that may be important for LPS−mammalian cell interactions at the gut level are still obscure. Here, we report on the full structure of the LPS isolated from one of the prominent species of the genus *Bacteroides*, *Bacteroides vulgatus*. The LPS turned out to consist of a particular chemical structure based on hypoacylated and *mono*-phosphorylated lipid A and with a galactofuranose-containing core oligosaccharide and an O-antigen built up of mannose and rhamnose. The evaluation of the immunological properties of this LPS on human *in vitro* models revealed a very interesting capability to produce anti-inflammatory cytokines and to induce a synergistic action of MD-2/TLR4- and TLR2-mediated signaling pathways.

Gut Microbiota

LPS structure

Human *in vitro* models

Anti-inflammatory cytokines
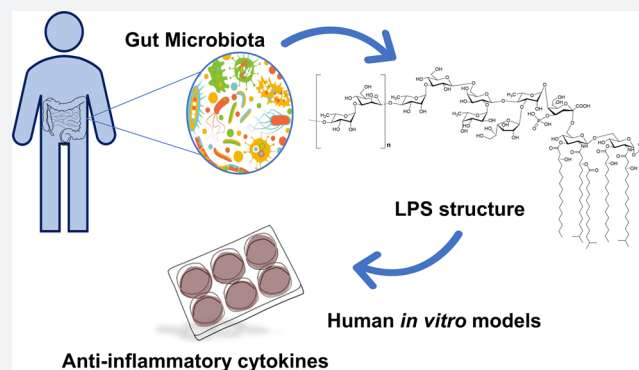
■ INTRODUCTION

The gastrointestinal tract is in incessant contact with microorganisms, collectively defined as "microbiota", which have profound impacts on the host immune system. The crosstalk between microbiota and the immune system at the level of the gut mucosa is crucial as it not only enables the tolerance of commensal microbes but also allows the immune system to recognize and fight pathogens thus preventing microbial invasion and infection.[1,2] The nature of the microbial signals and the cellular mechanisms underlying such host−microbe interactions are still enigmatic and need further studies.

Innate immune recognition of microbes relies on the detection of conserved microbial structures, known as "microbe-associated molecular patterns" (MAMPs) such as lipopolysaccharides (LPSs), whose detection by the host immune system is at the basis of infection, inflammation, or symbiosis via an intracellular signaling.[3,4] LPSs, the main constituents of the Gram-negative outer membrane, have a general structural architecture built up of three structural domains: a glycolipid portion termed lipid A, and a heteropolysaccharide composed of the core oligosaccharide (core OS) and the O-polysaccharide moiety (or O-chain).[5,6] In

mammals, the lipid A portion is recognized by the innate immunity receptor complex built up of myeloid differentiation protein-2 (MD-2) and Toll-like receptor 4 (TLR4).[7] It is widely attested that the immunopotential of an LPS is correlated to its fine structure; namely, defined LPS molecules act as agonists of the MD-2/TLR4 complex, triggering the immune response culminating in production of proinflammatory cytokines. Nevertheless, some other LPSs act as antagonist agents by preventing the binding of toxic LPS to the receptor complex, therefore inhibiting or limiting the dangerous effects on infected cells.[8]

In this context, a still pending key question is how the molecular interactions between LPS and its receptors, and the subsequent signaling pathways, lead to disease vs commensalism or even mutualism. Since it is widely accepted that the
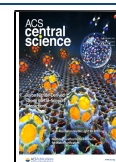
innate immune responses, upon stimulation by LPS, are finely tuned by its chemical composition,[3−8] one can envision that commensal gut microbiota express "modified" LPS structures well tolerated/not rejected by the host immune system.[9] Therefore, a crucial point to be addressed is what commensal gut microbiota LPS looks like. To shed light on this, we have started a program aimed at looking for the structure to function relationship of LPS from gut microbiota. First we focused our attention on *Bacteroides*, the prominent Bacteroidetes representative in the gastrointestinal tract of the healthy American and Western European population, whose members can be considered as commensal, mutualist, or even pathobiont microorganisms.[10] *Bacteroides* surface structures have been shown to exert immunomodulatory effects. Examples are given by the capsular polysaccharide component from *Bacteroides fragilis*[11,12] but also the LPS from *Bacteroides dorei* that in a study by Vatanen et al. was shown to promote immunological tolerance.[13] Recently, we demonstrated that *Bacteroides vulgatus* strain mpk, commensal of murine intestine, exerts strong immune-modulating properties leading to prevention of colitis-induction in several mouse models for experimental colitis.[14−16] Furthermore, we showed that its isolated LPS (LPS$_{Bv}$) does not induce expression of proinflammatory cytokines but actively induces hyporesponsiveness toward subsequent LPS-stimuli in CD11c+ cells in murine *in vitro* systems,[17] thereby fairly merging properties of TLR4 antagonists and agonists. Therefore, we proposed LPS$_{Bv}$ acting as a "weak agonist" concerning its interaction with the murine MD-2/TLR4 receptor complex.[17] Importantly, in the same work we also proved that the administration of purified LPS$_{Bv}$ reestablishes intestinal immune homeostasis in a mouse model for experimental colitis and correlated these health-promoting effects to the weak agonistic properties of this LPS exploited through induction of a special type of LPS tolerance in intestinal lamina propria CD11c+ cells, via the MD-2/TLR4 receptor complex axis.[17] Given that the administration of the sole LPS$_{Bv}$ in mice caused the restoring of the homeostasis in intestine after severe inflammation, this phenomenon must of course be attributed to its chemical structure, and therefore, we have decided to establish the full structure of its LPS.

Here, we report on the full characterization of the LPS$_{Bv}$ chemical structure achieved by the combined use of chemical, spectroscopic, and spectrometric techniques. Puzzled by the immunological properties of LPS$_{Bv}$ observed in murine systems, we wondered whether the observed activity could be mirrored in human *in vitro* systems. Therefore, we also evaluated the impact of LPS$_{Bv}$ on the human innate immune system by using HEK cell lines, human macrophages, and dendritic cells and discovered that to an intriguing chemical structure corresponded an equally intriguing immunological behavior.

◼ STRUCTURAL CHARACTERIZATION OF *B. VULGATUS* LPS: PURIFICATION AND CHEMICAL ANALYSES

In order to define the full structure of the LPS$_{Bv}$, a multidisciplinary approach was employed. In detail, a set of chemical analyses, on both intact and isolated LPS domains, was executed, furnishing the chemical composition of each LPS moiety.

LPS material was extracted from lyophilized bacterial cells by the hot phenol/water procedure.[18] The extracted LPS underwent an enzymatic digestion by DNase, RNase, and proteases in order to remove cell contaminants. A further step of purification by size-exclusion chromatography and ultracentrifugation was also performed. The nature and purity of the LPS$_{Bv}$ was determined by SDS-PAGE analysis after silver nitrate gel staining,[19] disclosing the smooth nature of the extracted LPS, as proven by the ladderlike pattern in the upper part of the gel indicating the occurrence of high-molecular-weight species, i.e., the O-chain moiety (Figure S1a). In parallel, no bands were visible in an additional SDS-PAGE analysis followed by Coomassie Brilliant Blue gel staining (Figure S1b) which was indicative of the absence of any contaminating protein/lipoprotein in the isolated LPS material. Furthermore, the Micro BCA protein assay has been also executed disclosing a protein content of less than 1% (i.e., ≤0.8 μg/mL) in the presence of 2% SDS as requested by manufacturer protocol to remove most of the well-known lipid interferences (Figure S1c).[20,21] However, it should be noted that the obtained value (≤0.8 μg/mL) (Figure S1c) was close to the lower limit of detection of the Micro BCA protein assay. For this reason (being close to the lower limit of detection) and due to the presence of lipids (i.e., the lipid A moiety), there are significant overestimations of the actual protein content (if any). In addition, as reported, the 2% SDS treatment remove only 70−80% of the lipid interferences.[20,21]

Chemical analyses[22−24] executed on pure LPS revealed the presence of terminal, 4-substituted and 3,4-disubstituted L-rhamnopyranose (L-Rha*p*), terminal L-fucopyranose (L-Fuc*p*), terminal galactofuranose (D-Gal*f*), 3-substituted D-mannopyranose (D-Man*p*), 3-substituted D-glucopyranose (D-Glc*p*), 2,6-disubstituted D-galactopyranose (D-Gal*p*), 6-substituted amino-D-glucopyranose (D-Glc*p*N), and 5-substituted Kdo. Fatty acid analysis[25] showed the occurrence of tetradecanoic acid (C14:0), pentadecanoic acid (C15:0), hydroxypentadecanoid acid (C15:0(3-OH)), hydroxyhexadecanoid acid (C16:0(3-OH)), and hydroxyheptadecanoic acid (C17:0(3-OH)), in full agreement with previously reported data by Hashimoto et al. on the structure of lipid A from *B. vulgatus* IMCJ 1204.[26]

◼ STRUCTURAL CHARACTERIZATION OF *B. VULGATUS* LPS: NMR OF THE SACCHARIDE PORTION

An aliquot of the pure LPS isolated from *B. vulgatus* mpk underwent a full deacylation[27] furnishing the complete LPS saccharide portion. The deacylated LPS fraction was then purified by gel permeation chromatography. Monosaccharide analysis of the isolated product confirmed the presence of the sugar residues detected in the intact LPS. The deacylated product was then analyzed by 1D and 2D NMR spectroscopy. A combination of homo- and heteronuclear 2D NMR experiments (DQF-COSY; TOCSY; NOESY; ROESY; ^{1}H, ^{13}C HSQC; ^{1}H, ^{13}C HMBC; and ^{31}P and ^{1}H, ^{31}P HSQC) was performed in order to elucidate the complete saccharide sequence of LPS$_{Bv}$. In detail, each spin system was assigned on the basis of the spin connectivity observed in both the double-quantum-filtered correlation spectroscopy (DQF-COSY) and the total correlation spectroscopy (TOCSY) spectra; each carbon atom was identified through the analysis of the heteronuclear single-quantum coherence (HSQC) spectrum. The anomeric configuration of all sugar units was defined by *intra*-residual NOE contacts, detectable in the nuclear Overhauser effect spectroscopy (NOESY) spectrum and the $^3J_{H-1,H-2}$ coupling constants from the DQF-COSY spectrum.

The assignment of the relative configuration of each sugar residue was obtained through the observation of the vicinal $^3J_{H,H}$ coupling constant values. The combined study of rotating-frame NOE spectroscopy (ROESY), NOESY, and HMBC (heteronuclear multiple-bond correlation spectroscopy) spectra allowed the characterization of the entire primary structure of the LPS saccharide part. Finally, ^{31}P and ^{31}P, ^1H HSQC experiments were pivotal to establish the location of the phosphate group decorating the LPS$_{Bv}$.

In the ^1H NMR spectrum (Figure 1) 11 anomeric signals from 11 spin systems were clearly identified (**A−L**; Table 1);
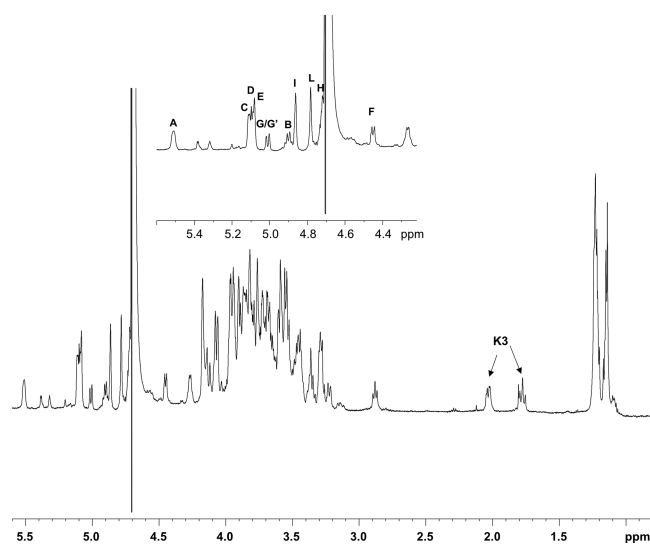

Figure 1. ^1H NMR of fully deacylated LPS$_{Bv}$. A zoom of the anomeric region is reported in the inset. Anomeric signals in the inset are as attributed in Table 1.

furthermore, the signals at δ_H 1.77 and 2.02 ppm were attributed to the H-3 methylene protons of the Kdo unit (**K**; Table 1). All the monosaccharide residues, except for **D**, were present as pyranose rings, according to both ^{13}C chemical shift values and the presence of long-range correlations between C-1/H-1 and H-5/C-5 observable in the ^1H, ^{13}C HMBC spectrum (for the Kdo residue between C-2 and H-6).[28] Conversely, residue **D** was present as a furanose ring as shown by the occurrence of low-field shifted ring carbon signals resonating around δ_C 82.0 ppm and anomeric carbon over δ_C 108 ppm and further confirmed by the *intra*-residual long-range H/C 1−4 correlations in the ^1H, ^{13}C HMBC spectrum.

Spin systems **A** (H-1 δ 5.50 ppm) and **B** (H-1 δ 4.90 ppm) were identified as the α-Glc$p$N and β-Glc$p$N of the lipid A moiety based on their H-2 proton signals, which correlated with two nitrogen-bearing carbon atoms at δ_C 54.3 and δ_C 55.6 ppm, respectively (Table 1, Figure S2). This hypothesis was also corroborated by the presence of an *inter*-residue contact between H-1 of **B** and H-6$_{a/b}$ of **A** observed in the NOESY spectrum (not shown). Furthermore, the occurrence of a correlation in the ^{31}P, ^1H HSQC spectrum (not shown), between the signal at δ 2.99 ppm and the anomeric proton signal of residue **A** (δ_H 5.50 ppm, Table 1, Figure S2), allowed the allocation of a phosphate group at such a position. Spin systems **C**, **G**, **G′**, and **I** were identified as α-rhamnopyranose residues as proven by the correlations, in the TOCSY spectrum, with the methyl group signals resonating at δ_H 1.23 and 1.24 ppm (δ_C 16.9 and 17.0 ppm; Table 1),

respectively. As mentioned above, the α-anomeric configuration was determined on the basis of the $^3J_{H-1,H-2}$ coupling constant values and the *intra*-residual NOE contact of H-1 with H-2, whereas the *manno* configuration was established by evaluation of $^3J_{H,H}$ coupling constant values.

Spin systems **D**, **E**, and **H** were attributed to *galacto*-configured sugar units. In detail, residue **D** (H-1 δ 5.07 ppm, Table 1), as stated above, was revealed to be a β-galactofuranose (anomeric carbon signal at δ 108.6 ppm, Table 1) based on its chemical shifts and *intra*-residual scalar and dipolar correlations. By contrast, spin system **H** (H-1 δ 4.72 ppm) was assigned to a β-galactopyranose, as proven by the chemical shift values of ring protons and the $^3J_{H,H}$ ring coupling constants; furthermore, the large $^3J_{H-1,H-2}$ values and the NOE correlations of H-1 with H-3 and H-5 were indicative of the β-anomeric configuration. The *galacto*-configured sugar residue **E** (H-1 δ 5.09 ppm) was identified as an α-fucopyranose as shown by the correlations, in the TOCSY spectrum, with the methyl proton signal at δ_H 1.14 ppm (δ_C 16.2 ppm) and the $^3J_{H-1,H-2}$ coupling constant values that confirmed the α-anomeric configuration.

Spin system **F** (H-1 δ 4.47 ppm) was assigned to a β-glucopyranose as indicated by the large $^3J_{H,H}$ ring coupling constants and the chemical shift values of ring protons, in agreement with the *gluco*-configuration of pyranose rings (Table 1). Moreover, the large $^3J_{H-1,H-2}$ values, together with the NOE contacts of H-1 with H-3 and H-5, were diagnostic of the β-anomeric configuration. Finally, spin system **L** (H-1 δ 4.78 ppm) was attributed to a β-mannopyranose residue, as proven by the small $^3J_{H-1,H-2}$ and $^3J_{H-2,H-3}$ values, diagnostic of a H-2 equatorial orientation, whereas the *intra*-residual correlations between H-1 and H-5 in the NOESY and ROESY spectra allowed the β configuration assignment. The assignment of the Kdo unit (**K**) was achieved starting from the diastereotopic methylene signal, and its anomeric α-configuration was assigned on the basis of the chemical shift values of H-3 (δ 1.77/2.02 ppm, Table 1), and of the $^3J_{H-7,H8a}$ and $^3J_{H-7,H-8b}$ coupling constants.[28,29] Moreover, the Kdo residue was phosphorylated at position O-4, due to the occurrence of a correlation with a signal at 1.64 ppm in the ^{31}P, ^1H HSQC spectrum (not shown).

The downfield shifted carbon signals were indicative of glycosylation at position O-6 of **A** and **B**, O-5 of **K**, O-3 and O-4 of **C**, O-2 and O-6 of **H**, O-3 of **F** and **L**, and O-4 of **I** and **G′**, whereas **D**, **E**, and **G** were terminal sugar residues, in full accordance with the methylation data. The analysis of the *inter*-residual NOE contacts (observable in both the NOESY and ROESY spectra) and the long-range correlations in the HMBC spectrum (Figure 2) allowed the defining of the complete sugar sequence of the LPS from *B. vulgatus* mpk. Starting from the lipid A disaccharide backbone, made up of residue **A** and **B**, this latter sugar unit was found to be substituted at position O-6 by the Kdo residue (**K**); this was further confirmed by the weak downfield shift of signal of C-6 of residue **B** (δ 61.3 ppm, Table 1), which is consistent with the α-(2→6) ketosidic linkage of Kdo with the β-GlcN of the lipid A. The Kdo unit was, in turn, substituted at position O-5 by the rhamnose residue **C**, as suggested by the long-range correlation between the anomeric proton signal of residue **C** and the carbon atom at δ 73.3 ppm (C-5, Table 1) of residue **K** (Figure 2). Rhamnose **C** was revealed to be substituted at both positions O-3 and O-4 by the *galacto*-configured sugar units **D** and **H**, respectively, as showed by the occurrence of the strong NOE

Table 1. ^{1}H, ^{13}C (*italic*) and ^{31}P (bold) Chemical Shift Values of the Saccharide Region of the LPS$_{Bv}$

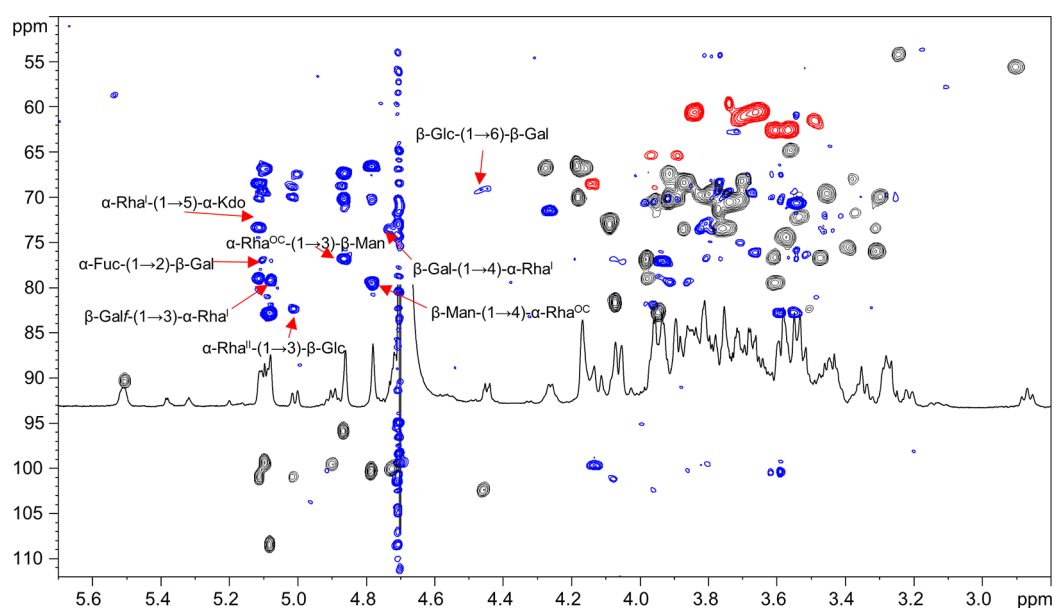| | chemical shifts (δ) | | | | | | | |
unit	1	2	3	4	5	6	7	8
A, 6-α-Glc*p*N	5.5	3.22	3.81	3.27	4.07	4.12/3.80		
	90.4	*54.3*	*69.9*	*70.1*	*73*	*68*		
	2.99							
B, 6-β-Glc*p*N	4.9	2.86	3.52	3.43	3.55	3.69/3.47		
	99.6	*55.6*	*72.3*	*69.8*	*74.5*	*61.3*		
C, 3,4-α-Rha*p* (α-Rha^{I})	5.11	4.16	3.96	3.85	3.85	1.23		
	101	*70.2*	*78.9*	*73.6*	*68.6*	*16.9*		
D, t-β-Gal*f*	5.07	4.06	3.96	3.92	3.72	3.56		
	108.6	*81.8*	*77*	*82.8*	*70.3*	*62.7*		
E, t-α-Fuc*p*	5.09	3.67	3.76	3.71	4.27	1.14		
	99.4	*68.3*	*71.4*	*73.2*	*66.9*	*16.2*		
F, 3-β-Glc*p*	4.47	3.29	3.48	3.36	3.36	3.82/3.62		
	102.5	*73.5*	*82.4*	*69.9*	*75.6*	*60.8*		
G, t-α-Rha*p* (α-Rha^{II})	5.01	3.93	3.81	3.34	3.96	1.22		
	100.8	*70.4*	*69.7*	*71.9*	*67.4*	*17*		
G′, 4-α-Rha*p* (α-Rha′^{II})	5	3.93	ND	3.58	3.88	1.22		
	100.8	*70.4*	*ND*	*79.4*	*67.5*	*17*		
H, 2,6-β-Gal*p*	4.72	3.45	3.75	3.8	3.71	3.93		
	100.2	*76.8*	*71.4*	*69.7*	*70.6*	*69*		
I, 4-α-Rha*p* (α-Rha^{OC})	4.86	3.9	3.94	3.58	3.89	1.22		
	99.7	*70.3*	*70.3*	*79.4*	*67.5*	*17*		
L, 3-β-Man*p*	4.78	4.17	3.58	3.54	3.29	3.82/3.64		
	100.3	*66.6*	*76.6*	*65*	*76.1*	*60.8*		
K, 5-α-Kdo*p*			1.77/2.02	4.15	4.07	3.68	3.96	3.95/3.86
			34.5	*67.2*	*73.3*	*70.5*	*70.2*	*65.6*
					1.64			

Figure 2. Zoom of the overlapped ^{1}H, ^{1}H, ^{13}C HMBC (blue) and ^{1}H, ^{13}C HSQC (black and red) NMR spectra. The key *inter*-residual long-range correlations involving sugar moieties (**A**−**L**) are indicated; letters are as in Table 1. Anomeric one-bond heteronuclear correlations were also reported in the spectrum.

contacts between H-1 of **D** and H-3 of **C** and between H-1 of **H** and H-4 of **C**. These glycosydic linkages were also confirmed by the observation of the respective long-range correlations in the HMBC spectrum (Figure 2). Residue **H**, in turn, was substituted by the α-Fuc **E** at position O-2 and by the β-Glc **F** at position O-6, as proven by the long-range correlations between the H-1 of **E** and the C-2 signal of **H**,

and H-1 of **F** and C-6 of **H** (Figure 2). This latter residue **F** turned out to be substituted at position O-3 by rhamnose **G**, as suggested by the long-range contact between the anomeric proton signal of **G** and the carbon atom signal at δ 82.4 ppm (C-3, Table 1) of β-glucose **F**. Interestingly, 2D NMR analysis allowed the identification of a second slight different glycoform of rhamnose **G**, referred to here as **G′**, differing for the
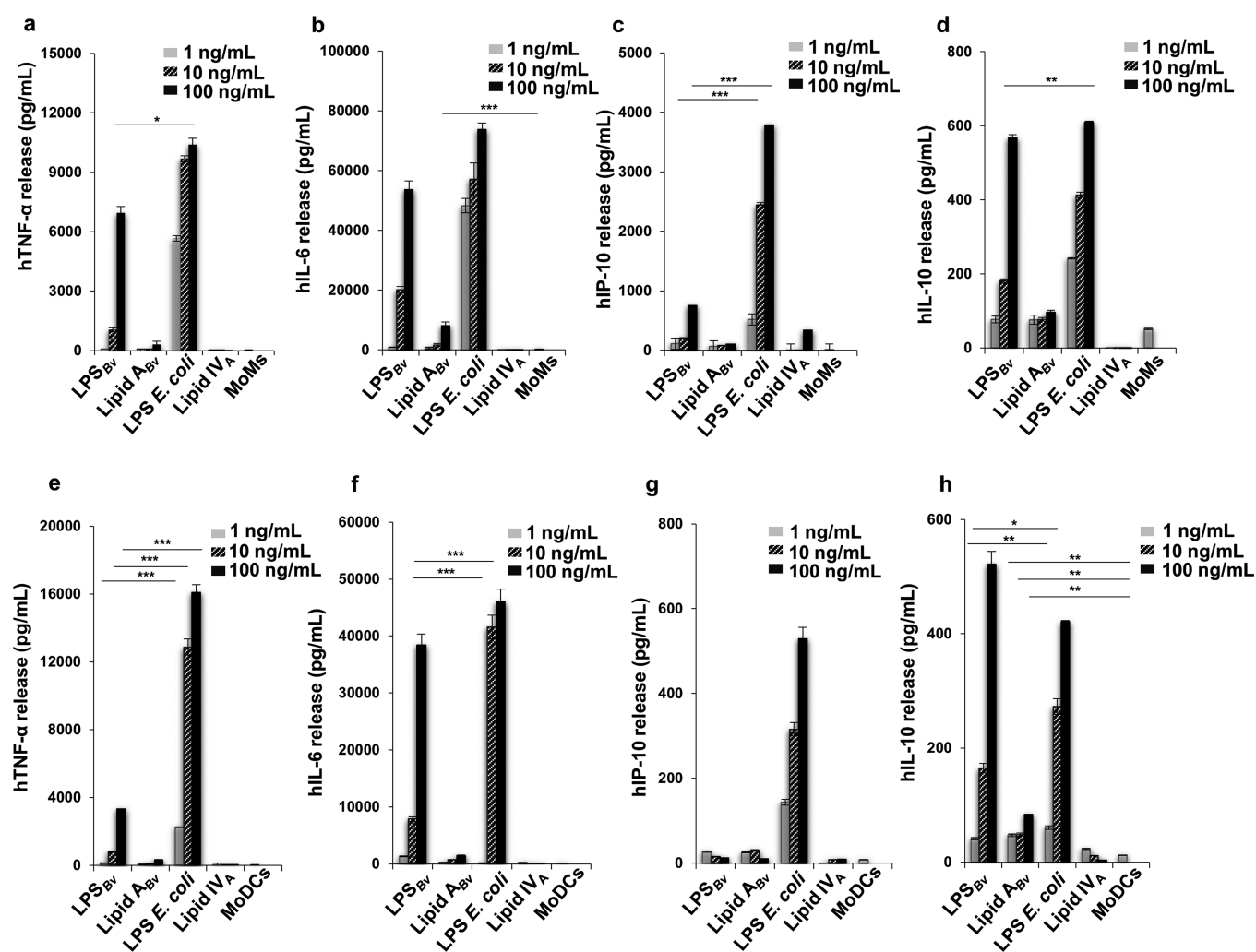
presence of a glycosylated position, namely, position O-4 (Table 1). Sugar units **I** and **L** were attributed to the components of the disaccharide repeating unit of the O-chain moiety as demonstrated by the long-range correlation of the anomeric proton signal of β-Man **L** with the carbon atom signal C-4 of α-Rha^{OC} **I** (Figure 2); further on, an HMBC correlation between the anomeric proton signal of **I** and C-3 of β-Man **L** was also clearly visible. These data were in full agreement with the LPS O-chain repeating unit previously elucidated by Hashimoto et al.[26] Finally, we were also able to establish the biological repeating unit; in fact, residue **G′**, assigned to a 4-substituted α-Rha, was identified as the sugar likely connecting the O-chain moiety to the core region, as proven by the long-range correlation between H-1 of **L** and C-4 of **G′** (Figure 2). This hypothesis was also confirmed by mass spectrometry (MS) and MS^2 data (see below).

All the above information taken together allowed the establishing of the complete structure of the fully deacylated LPS$_{Bv}$ as sketched below:

STRUCTURAL CHARACTERIZATION OF *B. VULGATUS* LPS: MASS SPECTROMETRY ANALYSIS

The fully deacylated LPS$_{Bv}$ was also analyzed by electrospray ionization (ESI) mass spectrometry (MS). The corresponding spectrum is reported in Figure S3a. The detailed investigation of the double and triple charged ions in the spectrum in the mass range m/z 400−1130 allowed the determination of the fine structure of the LPS saccharide domain. In detail, the spectrum showed three main signal clusters (**M1**−**M3**) of double charged ions (m/z 821.3, 975.4, and 1129.4, Figure S3a and Table S1) originating from the monoisotopic molecules with a mass of 1644.47, 1952.58, and 2260.69 (calculated molecular masses 1644.6, 1952.8, and 2260.8 Da), respectively, differing by 308 u, which corresponded to the mass of an O-chain repeating unit (RU) built up of a hexose and a deoxyhexose, thus in full agreement with the NMR data. Briefly, **M1** (the most abundant species) and **M2** contained one and two O-chain RU, respectively, whereas **M3** possessed three O-chain RU. Interestingly, the main peak m/z 667.3 was attributed to the double charged ion originating from the monoisotopic mass of 1336.36 (calculated molecular mass 1336.6 Da) which is consistent with an oligosaccharide composed of two hexosamines, one Kdo, two hexoses, two deoxyhexoses, and two phosphates. The structural sequence of the core OS was also corroborated by the ESI-MS^2 investigation executed on precursor ion 1336.36 which is reported in Figure S3b. The spectrum showed the occurrence of a daughter ion at m/z 419.2 (**Y$_2$**) originating from the monoisotopic mass 420.11 (calculated molecular mass 420.2 Da) assignable to the *mono*-phosphorylated diglucosamine backbone of the lipid A. Moreover, the daughter ion at m/z 915.4 (**B$_3$**) relative to a mass of 916.24 (calculated mass 916.4 Da) was attributed to the oligosaccharide fragment made up of one Kdo, one phosphate, two hexoses, and two deoxy-hexoses. Finally, the ESI-MS spectrum revealed also the occurrence of the two double charged ions at m/z 627.3 and 748.3 relative to the monoisotopic masses 1256.39 and 1498.41 (calculated

molecular masses 1256.6 and 1498.6 Da), respectively, which matched with the above-described core OS minus a phosphate group (1256.39) or carrying a further hexose unit (1498.41). Therefore, all above-mentioned MS and MS^2 data were in full accordance with the NMR structural elucidation of the saccharide moiety of the LPS$_{Bv}$.

In order to define also the structure of the glycolipid portion of the LPS$_{Bv}$, an aliquot of pure LPS underwent a mild acid hydrolysis in order to selectively cleave the acid-labile linkage between the Kdo and the β-GlcN unit and to isolate the lipid A fraction. After purification, this latter was then analyzed by MALDI MS. The MALDI MS spectrum (Figure S4), acquired in negative polarity, matched perfectly with the MS analysis executed by Hashimoto et al.[26] In detail, a high heterogeneity of lipid A species was immediately apparent as demonstrated by the occurrence of two clusters of signals differing in the number of the fatty acid chains (Figure S4). Moreover, each of these groups of ions was characterized by the presence of mass differences that can be explained with the presence of lipid A species differing in the fatty acid chain length. In detail, the most intense cluster of ions in the mass range m/z 1617−1717 Da (Figure S4) was consistent with *mono*-phosphorylated penta-acylated lipid A species whose fatty acid distribution and composition, for instance for the ion peak at m/z 1688.28, was determined as two C17:0(3-OH) as *N*-linked acyl chains, two C16:0(3-OH) as primary *O*-linked fatty acids, and C15:0 as a secondary *O*-acyl substitution. The less intense cluster of ions visible in the mass range m/z 1385−1479 Da (Figure S4) was attributed to *mono*-phosphorylated tetra-acylated lipid A species with the main ion peak at m/z 1436.02 assigned to a lipid A possessing the above-mentioned fatty acid distribution and composition but lacking one primary *O*-linked C16:0(3-OH).

Therefore, the overall data led to the delineation of the full structure of LPS$_{Bv}$ as sketched in Figure 3. Moreover, a first indication of the 3D perspective of the dynamic behavior in water of both the tetra- and penta-acylated forms of LPS$_{Bv}$ is reported in Figures S5−S7.

Figure 3. Complete structure of the LPS from *B. vulgatus* mpk. The lipid A is heterogeneous, being composed of a mixture of penta- and tetra-acylated *mono*-phosphorylated species. The dotted lines indicate the nonstoichiometric substitution. The O-chain repeating unit is indicated in square brackets.

Figure 4. Cytokine and chemokine release induced by LPS_{Bv} and lipid A_{Bv} in MoMs and MoDCs. Release of TNF-α (a, e), IL-6 (b, f), IP-10 (c, g), and IL-10 (d, h) in cell free supernatants of MoMs and MoDCs, respectively. Untreated cells are the negative control in these experiments. *$p <$ 0.05, **$p <$ 0.01, ***$p <$ 0.001.

ACTIVATION OF PERIPHERAL BLOOD-MONOCYTE-DERIVED MACROPHAGES AND OF PERIPHERAL BLOOD-MONOCYTE-DERIVED DENDRITIC CELLS BY *B. VULGATUS* LPS AND LIPID A

Once the structure was defined at a molecular level, we then passed to the immunological evaluation of LPS_{Bv} and its isolated lipid A portion (Lipid A_{Bv}) on human peripheral blood-monocyte-derived macrophages (MoMs) and on peripheral blood-monocyte-derived dendritic cells (MoDCs). LPS_{Bv} and lipid A_{Bv} were used to stimulate MoMs and MoDCs at the concentration of 1, 10, and 100 ng/mL. The agonistic hexa-acylated *Escherichia coli* O111:B4 LPS and the synthetic antagonist tetra-acylated lipid IV_A at the same concentration as above were used as controls. Untreated cells were considered the negative control in all the experiments. The release of cytokines tumor necrosis factor-α (TNF-α) (Figure 4a,e), interleukin-6 (IL-6) (Figure 4b,f), the chemokine IFN-γ-inducible protein-10 (IP-10) (Figure 4c,g), and the interleukin-10 (IL-10) (Figure 4d,h) were quantified by ELISA after 12 h of stimulation. The choice has fallen on these cytokines/chemokines as they are the most representative to demonstrate the inflammatory (TNF-α and IL-6) and anti-

inflammatory (IL-10) response following an LPS stimuli. Importantly, it is known that, following the recognition of LPS by TLR4, two signaling pathways mediated by the adaptor molecules MyD88 and TRIF, respectively, are triggered. Both pathways lead to the activation of the nuclear factor-κB (NF-κB) and the production of the proinflammatory mediators, while the only TRIF pathway promotes the production of type I interferon and the interferon-related cytokines/chemokines, such as the chemokine IP-10.[30] Therefore, the measurement of this chemokine was chosen to assess whether LPS_{Bv} can activate the TRIF pathway in addition to the MyD88 pathway.

In MoMs the amount of TNF-α triggered by LPS_{Bv} stimulation at 100 ng/mL was significantly reduced with respect to that of *E. coli* LPS at the same concentration ($p <$ 0.5) but comparable to that of *E. coli* LPS at 10 ng/mL (Figure 4a). Likewise, a similar trend was observed for the cytokine IL-6 (Figure 4b) as at the concentration of 100 ng/mL no significant difference was detected with *E. coli* LPS. The chemokine IP-10 yield triggered by 100 ng/mL of LPS_{Bv} was appreciable (Figure 4c) but significantly lower ($p <$ 0.001) than that of *E. coli* LPS at the same and minor concentration (10 ng/mL). Finally, upon stimulation with 100 ng/mL LPS_{Bv} or *E. coli* LPS, IL-10 production (Figure 4d) was comparable while at 10 ng/mL the difference between these values was
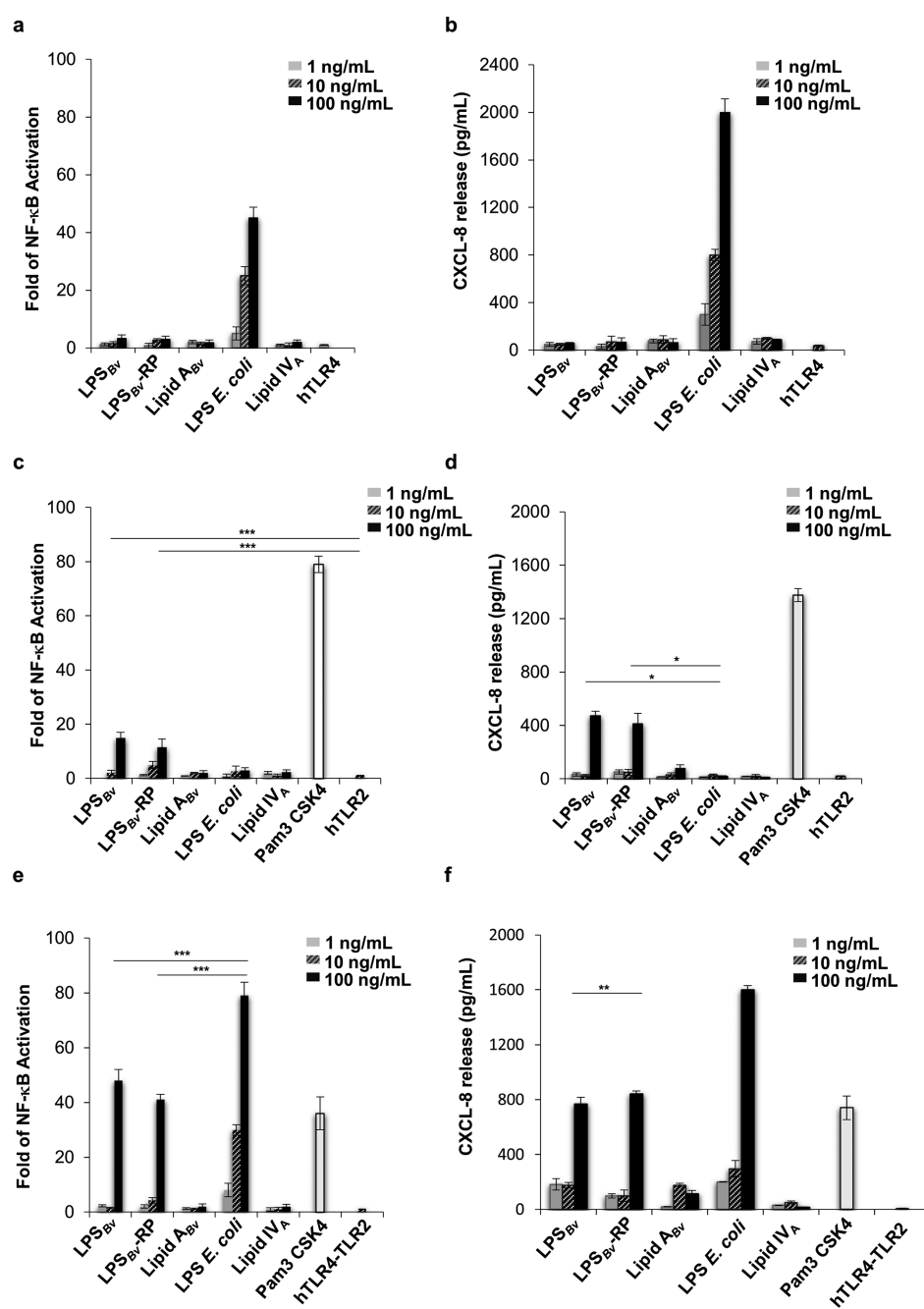
Figure 5. Analysis of the immunopotential of LPS_{Bv}, LPS_{Bv}-RP, and lipid A_{Bv}. HEK293 cells expressing hTLR4/MD2-CD14 (a, b) or hTLR2 (c, d) or hTLR4/MD2-CD14 and hTLR2 (e, f) were treated with LPS_{Bv}, LPS_{Bv}-RP, or lipid A_{Bv}, with *E. coli* LPS, with lipid IV_A at the concentration of 1, 10, and 100 ng/mL, or with TLR2 agonist Pam3 CSK4 (500 ng/mL) (c−f). Untreated cells were the negative control in these experiments. Fold of NF-κB activation in HEK293 hTLR4/MD2-CD14 (a), HEK293 hTLR2 (c), and HEK293 hTLR4/MD2-CD14 hTLR2 (e). Release of CXCL-8 release supernatants of HEK293 hTLR4/MD2-CD14 (b), HEK293 hTLR2 (d), and HEK293 hTLR2 hTLR4 cells (f). *$p < 0.05$, **$p < 0.01$, ***$p < 0.001$.

highly significant ($p < 0.01$). Lipid A_{Bv} did not produce the release of the cytokines measured with the exception of IL-6 that was scantly but significantly produced ($p < 0.001$, for Lipid A_{Bv} vs untreated cells) at the concentration of 100 ng/mL (Figure 4b). As expected, no cytokine production was observed with lipid IV_A.

In MoDCs, LPS_{Bv} triggered the production of TNF-α (Figure 4e) which was significantly lower than that of *E. coli* ($p < 0.001$ for all concentrations LPS_{Bv} vs *E. coli* LPS). IL-6 (Figure 4f) was produced in small amount at 1 and 10 ng/mL ($p < 0.001$ for LPS_{Bv} at 1 and 10 ng/mL vs *E. coli* LPS at the

same concentrations) while at 100 ng/mL the two yields were comparable. No release of TNF-α and IL-6 was seen following lipid A_{Bv} stimulation at all the concentrations tested (Figure 4e,f). The chemokine IP-10 (Figure 4g) was poorly detectable upon stimulation with either LPS_{Bv} or lipid A_{Bv}. In line with the trend observed in MoMs, in MoDCs IL-10 (Figure 4h) release by LPS_{Bv} was lower than that elicited by *E. coli* LPS at 1 and 10 ng/mL ($p < 0.01$ and $p < 0.05$, respectively, for LPS_{Bv} vs *E.coli* LPS at the same concentrations) while at 100 ng/mL no statistical difference between the two values was found.

Likewise, lipid A_{Bv} elicited an exiguous but still detectable production of IL-10 ($p < 0.01$ for lipid A_{Bv} vs untreated cells).

Furthermore, we also measured via ELISA the release of IL-6, IL-10 (Figure S8), and IFN-α by MoDCs after stimulation with LPS_{Bv} and *E. coli* LPS at different time points. This analysis confirmed the lower capacity of LPS_{Bv} in eliciting the production of IL-6 and IL-10 compared to *E. coli* LPS; finally, the absence of any detection of IFN-α, in addition to the poor detectability of the chemokine IP-10 release, further demonstrated that the LPS_{Bv}-induced IL-10 release is not regulated by IFN type I dependent pathways.

Therefore, the findings in MoDCs consolidated those achieved in MoMs and highlighted the peculiar ability of the LPS_{Bv} to stimulate selectively the release of IL-6 and the anti-inflammatory cytokine IL-10. It is noteworthy that the LPS_{Bv} stimulates the production of a low amount of TNF-α compared to IL-10 release, in contrast to what is observed with *E. coli* LPS which induced a high yield of TNF-α. This result defined a peculiar immunological property of LPS_{Bv} which is able to promote an anti-inflammatory response rather than the inflammation.

■ ACTIVATION OF BONE MARROW MONOCYTE-DERIVED MACROPHAGES BY *B. VULGATUS* LPS AND LIPID A

We then continued to analyze whether LPS_{Bv} and lipid A_{Bv} showed the same ability to induce the above profile of cytokine yield also in murine bone marrow monocyte-derived macrophages (BMDMs), which is the common model to analyze the immunopotential of LPS. The release of TNF-α, IL-6, IP-10, and IL-10 (Figure S9a−d) was quantified after 12 h of stimulation by ELISA. In contrast to human cells, in BMDMs stimulated with LPS_{Bv} at all concentrations the TNF-α production (Figure S9a) was scant and significantly lower ($p < 0.001$, for LPS_{Bv} vs *E. coli* LPS at all concentrations) than that induced by *E. coli* LPS at all concentrations tested. Likewise, IL-6 (Figure S9b), IP-10 (Figure S9c), and IL-10 (Figure S9d) values were undetectable or scantly detectable ($p < 0.05$ for IL-10: LPS_{Bv} at 100 ng/mL vs untreated cells). Conclusively, human but not murine cells seemed to be particularly sensitive to the immunopotential of LPS_{Bv}.

■ ACTIVATION BY LPS_{BV} AND LIPID A_{BV} IN HEK293 CELL MODELS

To acquire major insights on the biological properties of LPS_{Bv} and lipid A_{Bv} we tested them in the model of HEK293 cell line stably transfected with the human CD14/MD-2/TLR4 complex. As above, LPS_{Bv} and lipid A_{Bv}, *E. coli* LPS, and the lipid IV_A were analyzed at the concentration of 1, 10, and 100 ng/mL. After 6 h, the activation of the nuclear factor-κB (NF-κB) (Figure 5a) and the production of chemokine (C-X-C motif) ligand 8 (CXCL-8 or IL-8) were measured (Figure S8b) as the most common read-outs used to evaluate the HEK293 cell activation upon LPS stimulation. As shown in Figure 5a, in HEK293 hTLR4 the level of NF-κB activation induced by LPS_{Bv} (100 ng/mL) roughly reached 7% compared to that of *E. coli* LPS at the same concentration while the cells were not responsive to lipid A_{Bv}. No CXCL-8 release was detected upon LPS_{Bv} and lipid A_{Bv} exposure (Figure 5b). At 10 and 100 ng/mL *E. coli* LPS stimulated high levels of NF-κB activation and CXCL-8 production, and no response was seen

upon stimulation with lipid IV_A, in accordance with the acylation degree.

These results did not clarify the immunopotential of LPS_{Bv} and its lipid A detected in MoMs and MoDCs. It can be argued that, in contrast to HEK293 hTLR4, which are cells that do not express the TLRs,[31] macrophages and dendritic cells show the full panel of TLRs. Therefore, another TLR like TLR2 could cooperatively work with the TLR4. In this context, the issue of TLR2 activation by LPS is very controversial.[32] However, very recently it has been reported that *Helicobacter pylori* LPS is able to activate TLR2,[33] underlining that some atypical LPS could show a TLR2-activating capacity. Therefore, we tried to understand whether LPS_{Bv} or lipid A_{Bv} could induce a TLR2 response. The HEK293 expressing hTLR2 were used to assess the immunologic impact of LPS_{Bv} and lipid A_{Bv} at the concentration of 1, 10, and 100 ng/mL as above. *E. coli* LPS and lipid IV_A were used in parallel. Pam_3CSK_4 (Pam3 CSK4) (500 ng/mL), a synthetic triacylated lipopeptide (LP), which mimics the acylated amino terminus of bacterial LP, represented the positive control for a TLR2 ligand. As expected, no activation of NF-κB (Figure 5c) and no CXCL-8 (Figure 5d) release were detected upon stimulation with *E. coli* LPS and lipid IV_A. LPS_{Bv} (100 ng/mL), but not lipid A_{Bv}, elicited a visible degree of NF-κB activation ($p < 0.001$ vs untreated cells). With LPS_{Bv} CXCL-8 production was consistent with NF-κB results ($p < 0.05$ for LPS_{Bv} vs *E. coli* LPS, both at 100 ng/mL), and lipid A_{Bv} triggered only a scant yield. As expected, Pam3 determined high NF-κB activation and CXCL-8 production. These results matched with our previous observation of a slight activation of TLR2 in murine TLR2-HEK cells in response to LPS_{Bv} stimulation.[17]

Then, HEK293 hTLR4 cells were transfected with hTLR2 and analyzed under the same conditions as above (Figure 5e,f) to evaluate the mutual influence of both TLRs (TLR4 plus TLR2) upon stimulation with LPS_{Bv} and lipid A_{Bv}. In contrast to the results in HEK293 hTLR4, activation of NF-κB and CXCL-8 release induced a certain degree of activation following stimulation with LPS_{Bv} (100 ng/mL) although they were significantly lower ($p < 0.001$ and $p < 0.01$ for NF-κB and CXCL-8, respectively: LPS_{Bv} vs *E. coli* LPS, both at 100 ng/mL) than those of *E. coli* LPS at the same concentration. As controls, HEK293 null cells or carrying pcDNA3, stimulated as HEK293 hTLR2 and HEK293 hTLR4 hTLR2 cells, did not trigger any NF-κB activation and CXCL-8 production (Figure S10).

Importantly, LPS preparations containing highly immunoactive contaminants, i.e., lipoproteins and phospholipids, that could be responsible for the observed TLR2-mediated signaling, have been previously reported.[34] Therefore, despite the extensive steps of purifications and the results of both the SDS-PAGE and the Micro BCA protein assay, we performed a further step of "repurification" of the LPS_{Bv} to eliminate possible lipoproteins present as previously described,[35,36] preceded by several washes with a mixture of chloroform−methanol (1:2, v/v) and chloroform−methanol−water (3:2:0.25, v/v) to remove traces of phospholipids possibly present. No detectable proteins were observed in the repurified LPS (LPS_{Bv}-RP) analyzed by Micro BCA protein assay (Figure S1c), which was then employed for immunological studies on HEK293 cell lines. As shown in Figure 5, immunological tests executed on HEK293 hTLR4, HEK293 hTLR2, and HEK293 hTLR4 hTLR2 showed a similar behavior between the LPS_{Bv}

and the repurified LPS (LPS$_{Bv}$-RP), thus further confirming that the LPS$_{Bv}$ actually activates the TLR2-mediated signaling.

■ COMPETITION TESTS OF LPS$_{BV}$ AND LIPID A$_{BV}$ WITH AGONISTIC LPS IN HEK293 CELL MODEL

Some underacylated lipid A and/or unusual LPS, containing, for example, long fatty acid chains, do show an inhibitory activity against endotoxically active LPS in human cells.[37−40] In line with this issue, we tested the ability of LPS$_{Bv}$ or Lipid A$_{Bv}$ to compete with the hexa-acylated, fully immunocompetent *E. coli* LPS to engage the hTLR4 mediated signaling. With this aim, HEK 293 hTLR4 cells were preincubated for 1 h with LPS$_{Bv}$ or lipid A$_{Bv}$ and stimulated with 10 and 100 ng/mL of *E. coli* LPS for 4 h (Figure S11a−d). NF-κB activation and CXCL-8 production were quantified after this time. Lipid IV$_A$ was used in parallel under the same conditions as for LPS$_{Bv}$ and lipid A$_{Bv}$ as a control of the inhibitory effect. Under these experimental conditions, LPS$_{Bv}$ and lipid A$_{Bv}$ did not significantly inhibit the activity of NF-κB upon *E. coli* LPS stimulation at all the concentrations tested, albeit the trend of NF-κB was reduced with respect to the only stimulation with *E. coli* LPS (Figure S11a,b). This kinetics was confirmed and strengthened with the CXCL-8 yield as lipid A$_{Bv}$ (1 and 10 ng/mL) plus *E. coli* LPS (10 ng/mL) reduced significantly the production of CXCL-8 of *E. coli* LPS (10 ng/mL) alone ($p <$ 0.01) (Figure S11c). Likewise, LPS$_{Bv}$ and Lipid A$_{Bv}$ (1 and 10 ng/mL) plus *E. coli* LPS (100 ng/mL) induced a lower release of CXCL-8 than *E. coli* LPS (100 ng/mL) alone ($p < 0.01$) (Figure S11d). As expected, lipid IV$_A$ showed an inhibitory activity on *E. coli* LPS for NF-κB and CXCL-8 production at all the concentrations tested ($p < 0.001$). Therefore, LPS$_{Bv}$ and lipid A$_{Bv}$ show a weak inhibitory activity toward *E. coli* LPS. These data are in agreement with the observation that LPS$_{Bv}$ is only a slight competitive inhibitor of *E. coli* LPS for binding to murine TLR4.[17]

■ DISCUSSION

The involvement of the LPS in the host-gut microbiota cross-talk is receiving a growing interest as it is shown to play a crucial role, depending on its fine structure, triggering or preventing inflammation by modulating the host immune responses. Different LPS structures are at the basis of such divergent activities, with gut commensal LPS exerting only weak immune inflammatory reactions. Within this frame, the structural characterization of LPS from gut microbiota will potentially provide peculiar chemical characteristics which will be surely related to interesting immunological properties.

In this study, we fully established the LPS structure isolated from *B. vulgatus* mpk, a member of the genus *Bacteroides* which is predominant in mouse and human microbiota and whose health-promoting effects in murine model systems were previously described.[17] Briefly, the lipid A resulted in a heterogeneous mixture of tetra- and penta-acylated species (Figure 3 and Figure S4) whose nature and distribution of the fatty acids were as previously reported.[26] This lipid A blend resulted in being essentially phosphorylated only at the reducing glucosamine unit, and no lipid A species with a higher acylation and/or phosphorylation degree have been detected. As for the saccharide portion, the core region was built up of a hexa-saccharide bearing a phosphorylated Kdo unit, in turn, substituted at position O-5 by a Rha$p$ residue. This latter was found to be a branched monosaccharide

bearing a β-Gal$f$ unit at its position O-3 and, at position O-4, a β-Gal$p$ unit. The latter was, in turn, disubstituted by α-Fuc$p$ and, finally, by a β-Glc$p$ which was established to be the residue substituted by the first rhamnose of the O-chain. The O-chain structure was built up of repeating units of β-Man$p$ and α-Rha$p$, in agreement with what was previously published[26] where we have further established the biological O-chain repeating unit which starts with α-Rha$p$. Notably, to the best of our knowledge, this is the first time that the full structure of an LPS from *Bacteroides* spp. is completely defined since so far only relatively little information and disjointed and partial structures are available concerning *Bacteroides* LPS saccharide domains.[9]

The investigation of the immunological properties of LPS$_{Bv}$ in human macrophages showed a weaker capability to elicit proinflammatory cytokine production than *E. coli* LPS. Therefore, similar to what was observed in murine *in vitro* systems, it is tempting to translate in human immune cells the hypothesis of LPS$_{Bv}$ as acting providing a basic anti-inflammatory intracellular transcription program, without exceeding a proinflammatory threshold, that could exert a "protective" role for the colonized host. In addition, our results showed that LPS$_{Bv}$ was able to highly stimulate the release of IL-10, a potent anti-inflammatory cytokine that restrains pathogenic inflammation in the gut. Nevertheless, LPS$_{Bv}$ promoted some production of the pleiotropic cytokine IL-6 whereas the proinflammatory cytokine TNF-α was only scantly stimulated. It might be speculated that LPS$_{Bv}$ plays a key role in the host immune responses by balancing the excessive inflammation potentially induced by IL-6 with the anti-inflammatory activity of IL-10. The resulting immune balance is crucial to drive optimal immune responses without causing an overexuberant inflammation at the level of intestinal mucosa where microbiota proliferate.[41]

The use of HEK cell lines transfected with TLR4 confirmed a weaker agonistic effect of LPS$_{Bv}$ compared to LPS from *E. coli*. In addition, HEK TLR2 cell lines showed a specific and significant interaction only with LPS$_{Bv}$. Interestingly, this interaction was upregulated by the coexpression of TLR4 and TLR2 on the HEK cell lines, showing a clear synergistic effect between the two TLRs in NF-κB activation and CXCL-8 production.

It is intriguing to speculate that the overall LPS$_{Bv}$ particular architecture might have a role in the MD-2/TLR4 complexation with the LPS itself and the following downstream signaling. Within this frame, it has been recently demonstrated that total LPS from fecal samples of healthy adult humans, mainly composed of Bacteroidetes species, has the capability to facilitate host tolerance of gut microbes by potently antagonizing the host TLR4 pathway.[42] Indeed, it is widely known that the immunogenicity, or the strength of the intracellular signaling, triggered by LPS via TLR4 is mostly mediated by the lipid A structure.[43] Indeed, a reduction in the number of the lipid A acyl moieties typically correlates with a decreased immunopotency of the LPS. Contextually, hypo-acylated lipid A forms are conserved across Bacteroidetes species,[44] as also confirmed by our data which are in agreement with previous reported information regarding the tendency of *Bacteroides* species to accumulate linear or branched fatty acids with 15−17 carbon atoms in their LPS lipid A moiety.[42,44,45] Furthermore, both 1- and 4′- phosphates on the lipid A disaccharide backbone were demonstrated to be important moieties for MD-2/TLR4 receptor complex activation.[4] Since

LPS$_{Bv}$ possesses only one phosphate at position 1 of the reducing glucosamine, this may also contribute to its weaker (compared to *E. coli* LPS) agonistic effects as a missing 4′-phosphate was demonstrated to result in a 100-fold reduction in endotoxic activity.[46] Moreover, it has been recently demonstrated that the enzyme LpxF, which is responsible for removing a single phosphate from the lipid A, is conserved across commensal Bacteroidetes and serves to enhance bacterial resistance to antimicrobial peptides, thus favoring bacterial resilience in the intestine.[47] Finally, recent studies revealed that not only do the the lipid A phosphorylation and acylation pattern determine LPS toxicity, but also the occurrence of either positive or negative charged groups, other than glucosamine backbone associated phosphates, can increase LPS immunopotency.[48] In this case, besides Kdo and reducing glucosamine-phosphate, LPS$_{Bv}$ contains no further charged groups either in the lipid A part or in the core OS.

Nevertheless, with this study we highlight the involvement also of TLR2 in the immunopotential of LPS$_{Bv}$. This is a fascinating aspect since it has been demonstrated that the TLR2 pathway establishes colonization for commensals of the human gut microbiota.[49] In this frame, although it has been demonstrated that some atypical LPSs are able to activate the TLR2 signaling pathway,[33] it is still unclear how TLR2 recognizes LPS. Given the controversial data about the presence of TLR2-stimulating contaminants in LPS preparations of *Bacteroides* spp., here we proved that the isolated LPS$_{Bv}$ (as well as LPS$_{Bv}$-RP) was devoid of any immunoactive contaminant, thus further confirming the ability of this LPS to activate the TLR2 signaling in human cells, as also previously observed for murine TLR2-HEK cells in response to LPS$_{Bv}$ stimulation.[17] How to relate this crucial point to the structure of LPS$_{Bv}$ will be a logical follow up of the present results. Within this context, under the structural point of view, the presence, in the inner part of the LPS core, of Gal*f*, which is known to be immunogenic to mammals, is surely an innovative signature for bacterial LPS. Indeed, the occurrence of five membered sugar rings in the LPS core OS is very rare, and to the best of our knowledge, it has only been found in an environmental *Shewanella*[50] strain as well as in the thermophilic bacterium *Thermomonas hydrothermalis*.[51] It is worth noting that particular bacterial hallmark monosaccharides, such as Gal*f*, that can be recognized by lectins of the eukaryotic innate immunity system whose role is yet to be identified, have been recently reported.[52−54] Indeed, we firmly believe that the combination of all the peculiar chemical features of the LPS$_{Bv}$ molecule influences its net effect on human immune cells, and on this ground, the role of the Gal*f* unit in LPS$_{Bv}$ immunological properties is intriguing and requires a future in-depth study at the molecular level. In support of our hypothesis, a recent work by Erturk-Hasdemir et al. (2019)[12] demonstrated that a covalently linked lipid anchor in polysaccharide A, the zwitterionic capsular polysaccharide of *B. fragilis*, was critical for the initiation of the anti-inflammatory immune response through the simultaneous activation of the TLR2 signaling (by the lipid anchor) and the Dectin-1 pathway (by the polysaccharide moiety). Similarly, we deem that the saccharide regions of LPS$_{Bv}$ heavily contribute and collaborate with the lipid A portion in dictating the innate immune signaling mechanisms leading to the activation of an anti-inflammatory response.

By this study we intended to provide the complete structure of a commensal bacterium LPS and start the search for molecular motifs that might be important for LPS−eukaryotic cell interactions at the gut level. We are not aware of whether this new structure is a "chemical paradigm" of the intestinal microbiota LPS since, so far, only very few chemical structures of intestinal commensals have been established.[9,55] Certainly, we can say that a thin border exists between the homeostatic balance maintained by commensal gut microbes and the war unleashed by bacterial pathogens invading gut mucosa. This thin line is, at least in part, chemically represented by the LPS structure which, in the case of commensals, responds to particular chemical requirements, such as peculiar fatty acids chemistry, location, and distribution and peculiar monosaccharide presence in the core region (i.e., Gal*f*). In this specific case, this chemical structure also has a different immunological behavior, i.e., the mild activating effect and the combined TLR2/TLR4 activation.

■ EXPERIMENTAL SECTION

Extraction, Purification, and "Repurification" of LPS from *B. vulgatus* mpk. Bacterial dried cells (5 g) were extracted through the hot phenol/water procedure.[18] The row LPS (300 mg) was checked by SDS-PAGE after gel silver staining[19] revealing a smooth-type LPS only in the water phase. In order to remove cell contaminants, an intensive enzymatic treatment by RNase (Roth), DNase (Roth), and Proteinase K (Roth) at 37 and 56 °C was executed, followed by exhaustive dialysis. In order to further purify the LPS material, several ultracentrifugation steps (4 °C, 100 000*g*, 24 h) and a gel-filtration chromatography were also performed. The SDS-PAGE followed by silver staining was repeated to check the degree of purity of the isolated LPS confirming the previous analysis. Furthermore, an additional SDS-PAGE followed by Coomassie Brilliant Blue (Sigma-Aldrich) gel staining to evaluate the presence of protein/lipoprotein contaminants was also executed. In both SDS-PAGE analyses, the purified LPS$_{Bv}$ was prepared at the desired concentration (1 mg/mL) and boiled for 10 min, and then, 0.5, 1, 2, 4, and 8 μL/well were loaded on a 13.5% SDS gel with a 5% stacking gel and separated using a mini-PROTEAN electrophoresis instrument (Bio-Rad Laboratories). Silver and Coomassie Brilliant Blue staining of the gels was executed according to the standard protocols.

In order to establish the protein content of the purified LPS$_{Bv}$, the Pierce Micro BCA protein assay (Thermo Scientific) has been performed following the manufacturer protocol, at an LPS concentration 100 times higher than the concentration used in the cellular experiments. Finally, the assay was repeated in the presence of 2% SDS as suggested by the manufacturer to remove the significant lipid interference.[20,21]

In order to further exclude the presence of any TLR2-stimulating contaminant in the LPS$_{Bv}$ preparation, an aliquot of LPS$_{Bv}$, previously treated to remove nucleic acids and proteins, dialyzed, ultracentrifuged, and chromatographed as described above, underwent several washes with a mixture of chloroform−methanol (1:2, v/v) and chloroform−methanol−water (3:2:0.25, v/v) currently employed to remove phospholipids. Once the organic solvents were removed completely, the sample was subjected to the "repurification" protocol by Hirschfeld et al.[36] to remove any traces of lipoproteins possibly contaminating the isolated LPS$_{Bv}$. The so-obtained LPS (LPS$_{Bv}$-RP) was analyzed through the Pierce Micro BCA protein assay (Thermo Scientific). Finally, LPS$_{Bv}$-RP and LPS$_{Bv}$

were both employed for the immunological tests. No unexpected or unusually high safety hazards were encountered in this work.

Chemical Analyses of LPS from *B. vulgatus* mpk. LPS$_{Bv}$ monosaccharide content was established by analysis of the acetylated *O*-methyl glycoside derivatives obtained by treatment with HCl/MeOH (1.25 M, 85 °C, 24 h) followed by an acetylation step with acetic anhydride in pyridine (85 °C, 30 min). The absolute configuration of each sugar unit was defined through the evaluation of the *O*-octylglycoside derivatives as previously described.[22] The sugar linkage pattern was determined by the Ciucanu method:[23,24] briefly, an aliquot of sample was suspended in DMSO to which NaOH in powder was added and then methylated with CH$_3$I, hydrolyzed with trifluoroacetic acid (4 M, 100 °C, 4 h), carbonyl reduced with NaBD$_4$, and acetylated with pyridine and acetic anhydride. The total fatty acid content was established on intact LPS by treating with HCl (4 M, 100 °C, 4 h) followed by NaOH (5 M, 100 °C, 30 min). The pH was adjusted to reach slight acidity. After extraction in chloroform, fatty acids were then methylated with diazomethane.[25] All chemical analyses were performed by means of a gas−liquid chromatography (GLC-MS) Agilent Technologies 6850A instrument equipped with a mass selective detector 5973N and a Zebron ZB-5 capillary column (Phenomenex, 30 m × 0.25 mm i.d., flow rate 1 mL/min, He used as carrier gas) and using the following temperature program: 140 °C/240 °C at 3 °C/min.

Isolation of the LPS$_{Bv}$ Saccharide Domain. An aliquot of pure LPS was treated with anhydrous hydrazine (2 mL), stirred at 37 °C for 90 min, cooled, poured into ice-cold acetone (20 mL), and allowed to precipitate. The precipitate was centrifuged (4000*g*, 30 min), washed with ice-cold acetone, dried, dissolved in water, and lyophilized. The *O*-deacylated product was then *N*-deacylated with 4 M KOH. The removal of salts was executed by gel-filtration chromatography on a Sephadex G-10 column (Pharmacia, 50 × 1.5 cm). The fully deacylated product was further purified on a Toyopearl TSK HW-50 instrument (Tosoh Bioscience).

NMR Spectroscopy. 1D and 2D ^{1}H NMR spectra were recorded on a Bruker 600 DRX instrument equipped with a cryoprobe. The solvent employed was D$_2$O, and the temperature was 298 K and pD 7. Spectra calibration was performed with internal acetone (δ_H 2.225 ppm, δ_C 31.45 ppm). ^{31}P NMR experiments were carried out with a Bruker DRX-400 spectrometer; aqueous 85% phosphoric acid was used as the external reference ($\delta = 0.00$ ppm). The double-quantum filtered phase sensitive correlation spectroscopy (DQF-COSY) experiment was carried out by using data sets of 4096 × 256 points. Total correlation spectroscopy (TOCSY) experiments were executed with spinlock times of 100 ms, using data sets ($t_1 \times t_2$) of 4096 × 256 points. Rotating frame Overhauser enhancement spectroscopy (ROESY) and nuclear Overhauser enhancement spectroscopy (NOESY) experiments were recorded by using data sets ($t_1 \times t_2$) of 4096 × 256 points and by using mixing times between 100 and 400 ms. In all homonuclear experiments the data matrix was zero-filled in both dimensions to give a matrix of 4 K × 2 K points and was resolution enhanced in both dimensions by a cosine-bell function before Fourier transformation. The determination of coupling constants was obtained by 2D phase sensitive DQF-COSY.[56,57] Heteronuclear single quantum coherence (^{1}H, ^{13}C HSQC) and heteronuclear multiple bound correlation (^{1}H, ^{13}C HMBC) experiments were recorded in ^{1}H-detection mode

by single-quantum coherence with proton decoupling in the ^{13}C domain using data sets of 2048 × 256 points. ^{1}H, ^{13}C HSQC was executed using sensitivity improvement and in the phase-sensitive mode using Echo/Antiecho gradient selection, with multiplicity editing during the selection step.[58] The ^{1}H, ^{13}C HMBC experiment was optimized on long-range coupling constants with the low-pass *J* filter to suppress one-bound connectivity, using gradient pulses for selection. A delay of 60 ms was employed for the evolution of long-range correlations. A long-range coupling constant value of 6 Hz was used. The data matrix in both heteronuclear experiments was extended to 2048 × 1024 points using forward linear prediction.[59]

Molecular Modeling. Computational studies and MD simulations of the following molecules were performed: LPS$_{Bv}$ lipid A molecules (TetraLipA and PentaLipA) and tetra- and penta-acylated LPS$_{Bv}$ (LPS$_{Bv}$-tetra and LPS$_{Bv}$-penta). The modeled 3D structures were in agreement with the NMR data as can be deduced from the monitoring of selected inter-residue distances (not shown).

Building of the Ligands. Compounds TetraLipA, PentaLipA, LPS$_{Bv}$-tetra, and LPS$_{Bv}$-penta were constructed using the Maestro interface.[60] The 3D coordinates of *E. coli* LPS from PDB ID 3FXI were used as a template. The resulting structures were minimized using the OPLS3 force field, water as a solvent, and steepest descent as the method of minimization, with a maximum of 10 000 iterations.

Parameter Derivation. Parameterization of new units was performed using Gaussian09[61] by optimizing the geometries with the 6-31G basis set at the Hartree−Fock level of theory. Charges were derived by applying the RESP methodology implemented in Antechamber, assigning the general Amber14 force field (GAFF) atom types.

Molecular Dynamics (MD) Simulations. All the MD simulations were carried out using Amber14.[62] Each compound was solvated with water molecules (TIP3 force field), and Na$^+$ counterions were added. Several steps of equilibration were performed before running the MD simulation. The first one consisted of 1000 steps of steepest descent minimization followed by 7000 steps of conjugate gradient minimization; a 100 kcal/(mol A^2) harmonic potential constraint was applied to the solute. In the four subsequent steps, the harmonic potential was progressively lowered, respectively, to 10, 5, and 2.5 kcal/(mol A^2)) for 600 steps of conjugate gradient minimization each time, and then, the whole system was minimized uniformly. In the following step, the system was heated from 0 to 100 K using the Langevin thermostat in the canonical ensemble (NVT) while applying a 20 kcal/(mol A^2) harmonic potential restraint on the proteins and the ligand. The next step heated up the system from 100 to 300 K in the isothermal−isobaric ensemble (NPT) under the same restraint condition as in the previous step. In the last step, the same parameters were used to simulate the system for 100 ps, but no harmonic restraint was applied. At this point, the system was ready for the production run, which was performed using the Langevin thermostat under NPT ensemble, at a 2 fs time step. A 100 ns trajectory was generated and further analyzed.

ESI MS and MS/MS Analysis. MS spectra of the saccharide part of LPS$_{Bv}$ were acquired on an amazon SL ion trap (IT) mass spectrometer with electrospray ionization (ESI) (Bruker Daltonics). The sample (75 µg) was dissolved in 50 µL of acetonitrile/water/formic acid solution (100:100:1, v/v/v) and analyzed in negative ion mode. The ion corresponding

to core OS (m/z 667.3) was analyzed by MS/MS. Source parameters were as follows: sample flow, 3 μL/min; ion source temperature, 200 °C; nitrogen flow, 5 L/min at a pressure of 8 psi. Spectra were scanned in the 200−2000 m/z range. He was used as the collision gas in the IT. The system was calibrated using ESI-L tuning mix (Agilent Technologies).

Isolation of the Lipid A Fraction from LPS$_{Bv}$. Isolation of lipid A was achieved by mild acid hydrolysis by using acetate buffer (1 mL, pH = 4.4) promoted by SDS (1 mg/mL) on ca. 20 mg of isolated LPS at 100 °C. The solution was extracted three times with CHCl$_3$/MeOH/H$_2$0 (100:30:30, v/v/v) and centrifuged (4 °C, 7000g, 15 min). The organic phase containing the lipid A was further purified by several washes with distilled water and then freeze-dried.

MALDI MS Analysis on Isolated A from LPS$_{Bv}$. Lipid A isolated after mild acid hydrolysis of LPS$_{Bv}$ was analyzed with a MALDI-TOF ultrafleXtreme spectrometer (Bruker Daltonics). 100 μg of lipid A was dissolved in 100 μL of milli-Q water after 10 min of incubation at 40 °C in the ultrasonic bath. 9H-pyrido(3,4)-indole (10 mg) was mixed with 1 mL of CHCl$_3$/MeOH (1:1, v/v), and 0.5 μL of the matrix was spotted onto the matrix. The sample was analyzed in reflectron, negative ion mode, scan range: m/z 700−3500. Instrument was calibrated within 1000−3150 Da mass range, using peptide mixture (Peptide Calibration Standard, Bruker Daltonics).

HEK 293 Cell Culture, Transfection, and Stimulation. The HEK293 cell line, stably transfected with human TLR4/MD2-CD14 (InvivoGen), was seeded into a 24-well plate at the concentration of 5×10^5 cells/mL. 48 h after seeding, the cells were transiently transfected through PolyFect transfection reagent (Qiagen) with a reaction mix containing 250 ng of Firefly luciferase reporter constructs, pGL3.ELAM.tk [harboring nuclear factor kappa B (NF-κB) promoter sequences], and 25 ng of *Renilla* luciferase reporter plasmid, pRLTK (as an internal control). For hTLR2, HEK293 cells or HEK293 cells hTLR4/MD2-CD14 were transfected through PolyFect transfection reagent with the plasmid pcDNA3-TLR2-YFP (pcDNA3-TLR2-YFP was a gift of Doug Bolenbock, Addgene plasmid 13016) and treated as above. The day after, the cells (HEK293 hTLR4/MD2-CD14, HEK293 hTLR2, or HEK293 hTLR4/MD2-CD14 hTLR2) were incubated with different concentrations of LPS$_{Bv}$, LPS$_{Bv}$-RP, or lipid A$_{Bv}$ (1, 10, and 100 ng/mL) or with purified *E. coli* LPS (LPS-EB ultrapure; InvivoGen) or with synthetic lipid IV$_A$ used at the same concentrations as above, for 6 h to analyze NF-κB activity (dual luciferase reporter assay system, Promega) and to measure CXCL-8 release (DuoSet R&D system). In the experiments including the TLR2 in addition to LPS$_{Bv}$, LPS$_{Bv}$-RP, and lipid A$_{Bv}$, Pam3 CSK4 (Pam3 CSK4) (InvivoGen) (500 ng/mL) was used as a positive control. Where necessary, HEK293 cells only or HEK293 cells pcDNA3 were exposed to LPSs and lipid A or Pam3 CSK4, as above. For the competition assay, HEK 293 hTLR4/MD2-CD14 cells were primed with 1, 10, and 100 ng/mL of LPS$_{Bv}$ or lipid A$_{Bv}$, or lipid IV$_A$ for 1 h and then exposed to *E. coli* LPS (10 and 100 ng/mL) for 4 h. After this time, NF-κB activity and CXCL-8 production were measured.

Human Macrophage and Dendritic Cell Isolation, Cultures, and Stimulation. Peripheral blood mononuclear cells (PBMCs) were isolated from buffy coats obtained by the blood bank of Sapienza University or Sanquin Blood bank, Amsterdam, The Netherlands, from healthy adult volunteers (blood donors) following written informed consent in

accordance with the Declaration of Helsinki. Each experiment included two buffy coats from two healthy adult volunteers and was carried out in triplicate.

For macrophages, PBMCs were obtained through a density gradient. CD14+ monocytes were isolated using the MACS microbead system (Miltenyi Biotec, Bergisch Gladbach, Germany). The monocytes were cultured for 6 days in RPMI 1640 (Lonza) supplemented with 10% heat-inactivated FBS (Euroclone Fetal Bovine Serum, GE Healthcare Life Sciences), 100 μM nonessential amino acids, 1 mM sodium pyruvate, 1000 U/mL penicillin, and 1000 U/mL streptomycin (all from Lonza) and 60 ng/mL GM-CSF (granulocyte-macrophage colony-stimulating factor) (Miltenyi Biotec) to obtain human macrophages (MoMs).

For dendritic cells, CD14+ monocytes were isolated using the MACS microbead system (Miltenyi Biotec, Bergisch Gladbach, Germany). The monocytes were cultured for 5 days in RPMI 1640 (Lonza) supplemented with 10% heat-inactivated FBS (HyClone Fetal Bovine Serum, GE Healthcare Life Sciences), 100 μM nonessential amino acids, 1000 U/mL penicillin, and 1000 U/mL streptomycin (all from Lonza), 20 ng/mL IL-4, and 50 ng/mL GM-CSF (both Miltenyi Biotec) to obtain immature human dendritic cells. MoDCs were characterized by immunostaining with CD11c, CD14, and CD80 (all from BD Pharmingen) through a flow cytometric analysis.

For MoMs and MoDCs stimulation, the cells were seeded in cell plates (2.5×10^5 cells/well for MoMs and 5×10^5 cells/well for MoDCs) and exposed to 1, 10, and 100 ng/mL of LPS$_{Bv}$ or lipid A$_{Bv}$, or lipid IV$_A$ or *E. coli* LPS used at the same concentrations for 12 h. Cell supernatants were then collected and processed for ELISA to measure the levels of TNF-α, IL-10, IL-6, and IP-10.

As for the time-course of IL-6 and IL-10 release by MoDCs, cells were stimulated with LPS$_{Bv}$ (10 ng/mL) after 1, 2, 4, 6, 8, and 24 h, and with 100 ng/mL after 1 and 24 h. Data are expressed as percentage of effect, and they are normalized over the MoDCs treated with LPS from *E. coli* (10 ng/mL at 24 h) set at 100%.

Bone Marrow-Monocyte-Derived Macrophage (BMDM) Isolation, Culture, and Stimulation. C57BL/6 mice were purchased from Charles River. BMDMs were derived from the bone marrow cells collected from 5 week old female mice, as already reported.[39] Animal studies were conducted according to protocols approved by the University of Rome La Sapienza and adhered strictly to the Italian Ministry of Health guidelines for the use and care of experimental animals. BMDMs were differentiated during 7 days in RPMI 1640 (Lonza), supplemented with 10% of heat-inactivated FBS (HycloneTM, Euroclone), 1% of L-glutamine (Lonza), 1% sodium pyruvate (Lonza), 1% NEAA (Lonza), 0.5% 2-ME (Gibco), and 40 ng/mL macrophage colony-stimulating factor (M-CSF; Miltenyi Biotec). BMDMs were seeded into 24-well plate (5×10^5 cells per well) and were incubated with different concentrations of LPS$_{Bv}$ or lipid A$_{Bv}$ (1, 10, and 100 ng/mL), *E. coli* LPS, or with lipid IV$_A$ at the same concentrations for 12 h. After this, cell supernatants were then collected and processed for ELISA to measure the levels of TNF-α and IL-10, IL-6, and IP-10.

ELISA Assay. Cytokine and chemokine concentrations were determined by commercially available ELISA kits (Duo Set Kit R&D systems or ThermoFisher Scientific IFN alpha

Human ELISA Kit). The absorbance was measured on a LT-4000 microplate reader (Labtech) (Hercules, CA).

Statistical Analysis. Data were presented as mean ± SD of at least 4 independent experiments (for human macrophages and dendritic cells, two donors for each experiment carried out in triplicate, as stated above). The statistical analysis has been carried out through GraphPad Prism software. For multiple group comparison the software used the multiple t test followed by Sidak−Bonferroni correction. Statistical significance was set at *$p \leq 0.05$.

■ ASSOCIATED CONTENT

Ⓢ Supporting Information
The Supporting Information is available free of charge at https://pubs.acs.org/doi/10.1021/acscentsci.0c00791.

Additional figures including staining images, assay results, NMR spectra, ESI-MS spectra, MALDI MS spectra, inter-residue distances, structures, and ELISA results (PDF)

■ AUTHOR INFORMATION

Corresponding Authors
Flaviana Di Lorenzo − *Department of Chemical Sciences and Task Force on Microbiome Studies, University of Naples Federico II, 80126 Naples, Italy*; Email: flaviana.dilorenzo@unina.it

Antonio Molinaro − *Department of Chemical Sciences and Task Force on Microbiome Studies, University of Naples Federico II, 80126 Naples, Italy*; orcid.org/0000-0002-3456-7369; Email: molinaro@unina.it

Authors
Molly D. Pither − *Department of Chemical Sciences, University of Naples Federico II, 80126 Naples, Italy*

Michela Martufi − *Department of Biology and Biotechnologies "C. Darwin", Sapienza-University of Rome, 00185 Rome, Italy*

Ilaria Scarinci − *Department of Biology and Biotechnologies "C. Darwin", Sapienza-University of Rome, 00185 Rome, Italy*

Joan Guzmán-Caldentey − *Department of Structural and Chemical Biology, Centro de Investigaciones Biológicas, CIB-CSIC, 28040 Madrid, Spain*

Ewelina Łakomiec − *Hirszfeld Institute of Immunology and Experimental Therapy, Polish Academy of Sciences, Wrocław 53-114, Poland*

Wojciech Jachymek − *Hirszfeld Institute of Immunology and Experimental Therapy, Polish Academy of Sciences, Wrocław 53-114, Poland*

Sven C. M. Bruijns − *Department of Molecular Cell Biology and Immunology, Amsterdam Infection & Immunity Institute and Cancer Center Amsterdam, Amsterdam UMC, Vrije Universiteit Amsterdam, Amsterdam 1081 HV, The Netherlands*

Sonsoles Martín Santamaría − *Department of Structural and Chemical Biology, Centro de Investigaciones Biológicas, CIB-CSIC, 28040 Madrid, Spain*; orcid.org/0000-0002-7679-0155

Julia-Stephanie Frick − *Institute of Medical Microbiology and Hygiene, University of Tübingen, 72076 Tübingen, Germany*

Yvette van Kooyk − *Department of Molecular Cell Biology and Immunology, Amsterdam Infection & Immunity Institute and Cancer Center Amsterdam, Amsterdam UMC, Vrije Universiteit Amsterdam, Amsterdam 1081 HV, The Netherlands*

Fabrizio Chiodo − *Department of Molecular Cell Biology and Immunology, Amsterdam Infection & Immunity Institute and Cancer Center Amsterdam, Amsterdam UMC, Vrije Universiteit Amsterdam, Amsterdam 1081 HV, The Netherlands*; orcid.org/0000-0003-3619-9982

Alba Silipo − *Department of Chemical Sciences and Task Force on Microbiome Studies, University of Naples Federico II, 80126 Naples, Italy*; orcid.org/0000-0002-5394-6532

Maria Lina Bernardini − *Department of Biology and Biotechnologies "C. Darwin", Sapienza-University of Rome, 00185 Rome, Italy*

Complete contact information is available at:
https://pubs.acs.org/10.1021/acscentsci.0c00791

Author Contributions
F.D.L., A.S., M.L.B., and A.M. conceived the study. F.D.L., A.S., S.M.S., F.C., W.J., M.L.B., and A.M. designed and executed the research and wrote the manuscript. All authors have given approval to the final version of the manuscript.

Notes
The authors declare no competing financial interest.

■ ACKNOWLEDGMENTS

■ DEDICATION
This paper is dedicated to Prof. Jesús Jiménez-Barbero for his 60th birthday.

■ ABBREVIATIONS
BCA, bicinchoninic acid; CXCL-8, chemokine (C-X-C motif) ligand 8; ESI MS, electrospray Ionization Mass spectrometry; Fuc, fucose; Gal, galactose; Glc, glucose; GLC-MS, gas−liquid chromatography mass spectrometry; HEK cells, human embryonic kidney cells; IL-6, interleukin-6; IL-8, interleukin-8; IL-10, interleukin-10; IFN-α, interferon-α; IP-10, IFN-γ inducible protein-10; Kdo, keto-deoxy-D-*manno*-octanoic acid; LPS, lipopolysaccharide; LPS$_{Bv}$, *B. vulgatus* LPS; MALDI MS, matrix-assisted laser desorption/ionization mass spectrometry; MAMP, microbe-associated molecular pattern; Man, mannose; MD-2, myeloid differentiation protein-2; MoDCs, peripheral blood-Monocyte-derived dendritic cells; MoMs, peripheral blood-monocyte-derived macrophages; NF-kB, nuclear factor-κB; NMR, nuclear magnetic resonance; OS, oligosaccharide; Rha, rhamnose; RU, repeating unit; SDS-PAGE, sodium dodecyl sulfate-polyacrylamide gel electrophoresis; TLR2, toll-like receptor 2; TLR4, toll-like receptor 4; TNF-α, tumor necrosis factor α

■ REFERENCES

(1) Sender, R.; Fuchs, S.; Milo, R. Revised Estimates for the Number of Human and Bacteria Cells in the Body. *PLoS Biol.* **2016**, *14* (8), No. e1002533.

(2) Wexler, A. G.; Goodman, A. L. An insider's perspective: *Bacteroides* as a window into the microbiome. *Nat. Microbiol.* **2017**, *2*, 17026.

(3) Whitfield, C.; Trent, M. S. Biosynthesis and export of bacterial lipopolysaccharides. *Annu. Rev. Biochem.* **2014**, *83*, 99−128.

(4) Molinaro, A.; Holst, O.; Di Lorenzo, F.; Callaghan, M.; Nurisso, A.; D'Errico, G.; Zamyatina, A.; Peri, F.; Berisio, R.; Jerala, R.; Jiménez-Barbero, J.; Silipo, A.; Martín-Santamaría, S. Chemistry of lipid A: at the heart of innate immunity. *Chem. - Eur. J.* **2015**, *21* (2), 500−19.

(5) Raetz, C. R.; Whitfield, C. Lipopolysaccharide endotoxins. *Annu. Rev. Biochem.* **2002**, *71*, 635−700.

(6) Di Lorenzo, F.; De Castro, C.; Lanzetta, R.; Parrilli, M.; Silipo, A.; Molinaro, A. Lipopolysaccharides as microbe-associated molecular patterns: A structural perspective. In *Carbohydrates in Drug Design and Discovery*; Jiménez-Barbero, J., Javier Canada, F., Martín-Santamaría, S., Eds.; Royal Society of Chemistry (RSC): London, UK, 2015; pp 38−63.

(7) Triantafilou, M.; Triantafilou, K. Lipopolysaccharide recognition: CD14, TLRs and the LPS-activation cluster. *Trends Immunol.* **2002**, *23*, 301−304.

(8) Akira, S.; Uematsu, S.; Takeuchi, O. Pathogen recognition and innate immunity. *Cell* **2006**, *124*, 783−801.

(9) Di Lorenzo, F.; De Castro, C.; Silipo, A.; Molinaro, A. Lipopolysaccharide structures of Gram-negative populations in the gut microbiota and effects on host interactions. *FEMS Microbiol. Rev.* **2019**, *43* (3), 257−272.

(10) Davenport, E. R.; Sanders, J. G.; Song, S. J.; Amato, K. R.; Clark, A. G.; Knight, R. The human microbiome in evolution. *BMC Biol.* **2017**, *15*, 127.

(11) Neff, C. P.; Rhodes, M. E.; Arnolds, K. L.; Collins, C. B.; Donnelly, J.; Nusbacher, N.; Jedlicka, P.; Schneider, J. M.; McCarter, M. D.; Shaffer, M.; Mazmanian, S. K.; Palmer, B. E.; Lozupone, C. A. Diverse intestinal bacterial contain putative zwitterionic capsuar polysaccharides with anti-inflammatory properties. *Cell Host Microbe* **2016**, *20*, 535−547.

(12) Erturk-Hasdemir, D.; Oh, S. F.; Okan, N. A.; Stefanetti, G.; Gazzaniga, F. S.; Seeberger, P. H.; Plevy, S. E.; Kasper, D. L. Symbionts exploit complex signaling to educate the immune system. *Proc. Natl. Acad. Sci. U. S. A.* **2019**, *116*, 26157.

(13) Vatanen, T.; Kostic, A. D.; d'Hennezel, E.; Siljander, H.; Franzosa, E. A.; Yassour, M.; Kolde, R.; Vlamakis, H.; Arthur, T. D.; Hämäläinen, A. M.; Peet, A.; Tillmann, V.; Uibo, R.; Mokurov, S.; Dorshakova, N.; Ilonen, J.; Virtanen, S. M.; Szabo, S. J.; Porter, J. A.; Lähdesmäki, H.; Huttenhower, C.; Gevers, D.; Cullen, T. W.; Knip, M.; Xavier, R. J. Variation in Microbiome LPS Immunogenicity Contributes to Autoimmunity in Humans. *Cell* **2016**, *165*, 842−853.

(14) Waidmann, M.; Bechtold, O.; Frick, J. S.; Lehr, H. A.; Schubert, S.; Dobrindt, U.; Loeffler, J.; Bohn, E.; Autenrieth, I. B. *Bacteroides vulgatus* protects against *Escherichia coli*-induced colitis in gnotobiotic interleukin-2-deficient mice. *Gastroenterology* **2003**, *125*, 162−177.

(15) Müller, M.; Fink, K.; Geisel, J.; Kahl, F.; Jilge, B.; Reimann, J.; Mach, N.; Autenrieth, I. B.; Frick, J. S. Intestinal colonization of IL-2 deficient mice with non-colitogenic *B. vulgatus* prevents DC maturation and T-cell polarization. *PLoS One* **2008**, *3*, No. e2376.

(16) Steimle, A.; Gronbach, K.; Beifuss, B.; Schäfer, A.; Harmening, R.; Bender, A.; Maerz, J. K.; Lange, A.; Michaelis, L.; Maurer, A.; Menz, S.; McCoy, K.; Autenrieth, I. B.; Kalbacher, H.; Frick, J. S. Symbiotic gut commensal bacteria act as host cathepsin S activity regulators. *J. Autoimmun.* **2016**, *75*, 82−95.

(17) Steimle, A.; Michaelis, L.; Di Lorenzo, F.; Kliem, T.; Münzner, T.; Maerz, J. K.; Schäfer, A.; Lange, A.; Parusel, R.; Gronbach, K.; Fuchs, K.; Silipo, A.; Öz, H. H.; Pichler, B. J.; Autenrieth, I. B.; Molinaro, A.; Frick, J. S. Weak Agonistic LPS Restores Intestinal Immune Homeostasis. *Mol. Ther.* **2019**, *27*, No. 1974.

(18) Westphal, O.; Jann, K. Bacterial lipopolysaccharides: extraction with phenol-water and further applications of procedure. *Carbohydr. Chem.* **1965**, *5*, 83−91.

(19) Kittelberger, R.; Hilbink, F. Sensitive silver-staining detection of bacterial lipopolysaccharides in polyacrylamide gels. *J. Biochem. Biophys. Methods* **1993**, *26*, 81−86.

(20) Kessler, R. J.; Fanestil, D. D. Interference by lipids in the determination of protein using bicinchoninic acid. *Anal. Biochem.* **1986**, *159* (1), 138−42.

(21) Morton, R. E.; Evans, T. A. Modification of the bicinchoninic acid protein assay to eliminate lipid interference in determining lipoprotein protein content. *Anal. Biochem.* **1992**, *204* (2), 332−4.

(22) Leontein, K. Assignment of absolute configuration of sugars by glc of their acetylated glycosides formed from chiral alcohols. *Carbohydr. Res.* **1978**, *62*, 359−362.

(23) Ciucanu, I.; Kerek, F. A simple and rapid method for the permethylation of carbohydrates. *Carbohydr. Res.* **1984**, *131*, 209−217.

(24) De Castro, C.; Parrilli, M.; Holst, O.; Molinaro, A. Microbe-associated molecular patterns in innate immunity: Extraction and chemical analysis of gram-negative bacterial lipopolysaccharides. *Methods Enzymol.* **2010**, *480*, 89−115.

(25) Rietschel, E. T. Absolute configuration of 3-hydroxy fatty acids present in lipopolysaccharides from various bacterial groups. *Eur. J. Biochem.* **1976**, *64*, 423−428.

(26) Hashimoto, M.; Kirikae, F.; Dohi, T.; Adachi, S.; Kusumoto, S.; Suda, Y.; Fujita, T.; Naoki, H.; Kirikae, T. Structural study on lipid A and the O-specific polysaccharide of the lipopolysaccharide from a clinical isolate of *Bacteroides vulgatus* from a patient with Crohn's disease. *Eur. J. Biochem.* **2002**, *269*, 3715−3721.

(27) Holst, O. Deacylation of lipopolysaccharides and isolation of oligosaccharide phosphates. *Methods Mol. Biol.* **2000**, *145*, 345−353.

(28) Birnbaum, G. I. Conformations of ammonium. 3-deoxy-D-manno-2-octulosonate (KDO) and methyl -and -ketopyranosides of KDO: X-ray structure and 1H NMR analyses. *J. Carbohydr. Chem.* **1987**, *6*, 17−39.

(29) Silipo, A.; Molinaro, A.; Comegna, C.; Sturiale, L.; Cescutti, P.; Garozzo, D.; Lanzetta, R.; Parrilli, M. Full Structural Characterisation of the Lipooligosaccharide of a *Burkholderia pyrrocinia* Clinical Isolate. *Eur. J. Org. Chem.* **2006**, *2006*, 4874−4883.

(30) Yamamoto, M.; Sato, S.; Hemmi, H.; Hoshino, K.; Kaisho, T.; Sanjo, H.; Takeuchi, O.; Sugiyama, M.; Okabe, M.; Takeda, K.; Akira, S. Role of adaptor TRIF in the MyD88-independent toll-like receptor signaling pathway. *Science* **2003**, *301* (5633), 640−3.

(31) Hornung, V.; Rothenfusser, S.; Britsch, S.; Krug, A.; Jahrsdorfer, B.; Giese, T.; Endres, S.; Hartmann, G. Quantitative expression of toll-like receptor 1−10 mRNA cellular subsets of human peripheral blood mononuclear cells and sensitivity to CpG oligodeoxynucleotides. *J. Immunol.* **2002**, *168*, 4531−7.

(32) Chandler, C. E.; Ernst, R. K. Bacterial lipids: powerful modifiers of the innate immune response. *F1000Research* **2017**, *6*, 1334.

(33) Chavarría-Velázquez, C. O.; Torres-Martínez, A. C.; Montaño, L. F.; Rendón-Huerta, E. P. TLR2 activation induced by *H. pylori* LPS promotes the differential expression of claudin-4, −6, −7 and −9 via either STAT3 and ERK1/2 in AGS cells. *Immunobiology* **2018**, *223* (1), 38−48.

(34) Hashimoto, M.; Waki, J.; Nakayama-Imaohji, H.; Ozono, M.; Hashiguchi, S.; Kuwahara, T. TLR2-stimulating contaminants in glycoconjugate fractions prepared from Bacteroides fragilis. *Innate Immun.* **2017**, *23* (5), 449−458.

(35) Manthey, C. L.; Vogel, S. N. Elimination of trace endotoxin protein from rough chemotype LPS. *J. Endotoxin Res.* **1994**, *1*, 84−91.

(36) Hirschfeld, M.; Ma, Y.; Weis, J. H.; Vogel, S. N.; Weis, J. J. Cutting edge: repurification of lipopolysaccharide eliminates signaling through both human and murine toll-like receptor 2. *J. Immunol.* **2000**, *165* (2), 618−22.

(37) Miller, S. I.; Ernst, R. K.; Bader, M. W. LPS, TLR4 and infectious disease diversity. *Nat. Rev. Microbiol.* **2005**, *3* (1), 36−46.

(38) Schromm, A. B.; Brandenburg, K.; Loppnow, H.; Moran, A. P.; Koch, M. H.; Rietschel, E. T.; Seydel, U. Biological activities of lipopolysaccharides are determined by the shape of their lipid A portion. *Eur. J. Biochem.* **2000**, *267* (7), 2008−13.

(39) Lembo-Fazio, L.; Billod, J. M.; Di Lorenzo, F.; Paciello, I.; Pallach, M.; Vaz-Francisco, S.; Holgado, A.; Beyaert, R.; Fresno, M.; Shimoyama, A.; Lanzetta, R.; Fukase, K.; Gully, D.; Giraud, E.; Martín-Santamaría, S.; Bernardini, M. L.; Silipo, A. *Bradyrhizobium* Lipid A: Immunological Properties and Molecular Basis of Its Binding to the Myeloid Differentiation Protein-2/Toll-Like Receptor 4 Complex. *Front. Immunol.* **2018**, *9*, 1888.

(40) Di Lorenzo, F.; Palmigiano, A.; Al Bitar-Nehme, S.; Sturiale, L.; Duda, K. A.; Gully, D.; Lanzetta, R.; Giraud, E.; Garozzo, D.; Bernardini, M. L.; Molinaro, A.; Silipo, A. The Lipid A from *Rhodopseudomonas palustris* Strain BisA53 LPS Possesses a Unique Structure and Low Immunostimulant Properties. *Chem. - Eur. J.* **2017**, *23* (15), 3637−3647.

(41) Pandiyan, P.; Bhaskaran, N.; Zou, M.; Schneider, E.; Jayaraman, S.; Huehn, J. Microbiome Dependent Regulation of Tregs and Th17 Cells in Mucosa. *Front. Immunol.* **2019**, *10*, 426.

(42) d'Hennezel, E.; Abubucker, S.; Murphy, L. O.; Cullen, T. W. Total lipopolysaccharide from the human gut microbiome silences Toll-Like Receptor signaling. *mSys* **2017**, *2* (6), No. e00046-17.

(43) Brandenburg, K.; Mayer, H.; Koch, M. H.; Weckesser, J.; Rietschel, E. T.; Seydel, U. Influence of the supramolecular structure of free lipid A on its biological activity. *Eur. J. Biochem.* **1993**, *218*, 555−563.

(44) Johne, B.; Olsen, J.; Bryan, K. Fatty acids and sugars in lipopolysaccharides from *Bacteroides intermedius Bacteroides gingivalis* and *Bacteroides loescheii*. *Oral Microbiol. Immunol.* **1988**, *3*, 22−27.

(45) Rokosz, A.; Meisel-Mikołajczyk, F.; Kot, K.; Mieszała, M.; Szponar, B.; Gamian, A. Analysis of fatty acids from lipopolysaccharides of *Bacteroides thetaiotaomicron* and Bacteroides fragilis. *Med. Dosw. Mikrobiol.* **2001**, *53* (2), 177−83.

(46) Rietschel, E. T.; Kirikae, T.; Schade, F. U.; Mamat, U.; Schmidt, G.; Loppnow, H.; Ulmer, A. J.; Zähringer, U.; Seydel, U.; Di Padova, F. Bacterial endotoxin: molecular relationships of structure to activity and function. *FASEB J.* **1994**, *8*, 217−225.

(47) Cullen, T. W.; Schofield, W. B.; Barry, N. A.; Putnam, E. E.; Rundell, E. A.; Trent, M. S.; Degnan, P. H.; Booth, C. J.; Yu, H.; Goodman, A. L. Antimicrobial peptide resistance mediates resilience of prominent gut commensals during inflammation. *Science* **2015**, *347*, 170−5.

(48) Di Lorenzo, F.; Kubik, Ł.; Oblak, A.; Lorè, N. I.; Cigana, C.; Lanzetta, R.; Parrilli, M.; Hamad, M. A.; De Soyza, A.; Silipo, A.; Jerala, R.; Bragonzi, A.; Valvano, M. A.; Martín-Santamaría, S.; Molinaro, A. Activation of Human Toll-like Receptor 4 (TLR4)/Myeloid Differentiation Factor 2 (MD-2) by hypoacylated lipopolysaccharide from a clinical isolate of Burkholderia cenocepacia. *J. Biol. Chem.* **2015**, *290* (35), 21305−19.

(49) Round, J. L.; Lee, S. M.; Li, J.; Tran, G.; Jabri, B.; Chatila, T. A.; Mazmanian, S. K. The Toll-like receptor 2 pathway establishes colonization by a commensal of the human microbiota. *Science* **2011**, *332* (6032), 974−7.

(50) Vinogradov, E.; Korenevsky, A.; Beveridge, T. J. The structure of the carbohydrate backbone of the LPS from *Shewanella putrefaciens* CN32. *Carbohydr. Res.* **2002**, *337*, 1285−1289.

(51) Di Lorenzo, F.; Paciello, I.; Fazio, L. L.; Albuquerque, L.; Sturiale, L.; da Costa, M. S.; Lanzetta, R.; Parrilli, M.; Garozzo, D.; Bernardini, M. L.; Silipo, A.; Molinaro, A. Thermophiles as potential source of novel endotoxin antagonists: the full structure and bioactivity of the lipo-oligosaccharide from *Thermomonas hydrothermalis*. *ChemBioChem* **2014**, *15*, 2146−2155.

(52) Wesener, D. A.; Dugan, A.; Kiessling, L. L. Recognition of microbial glycans by human intelectin-1. *Curr. Opin. Struct. Biol.* **2017**, *44*, 168−178.

(53) Wesener, D. A.; Dugan, A.; Kiessling, L. L. Recognition of microbial glycans by soluble human lectins. *Curr. Opin. Struct. Biol.* **2017**, *44*, 168−178.

(54) Chiodo, F.; Marradi, M.; Park, J.; Ram, A. F.; Penadés, S.; van Die, I.; Tefsen, B. Galactofuranose-coated gold nanoparticles elicit a pro-inflammatory response in human monocyte-derived dendritic cells and are recognized by DC-SIGN. *ACS Chem. Biol.* **2014**, *9* (2), 383−9.

(55) Naito, T.; Mulet, C.; De Castro, C.; Molinaro, A.; Saffarian, A.; Nigro, G.; Bérard, M.; Clerc, M.; Pedersen, A. B.; Sansonetti, P. J.; Pédron, T. Lipopolysaccharide from Crypt-Specific Core Microbiota Modulates the colonic epithelial proliferation-to-differentiation balance. *mBio* **2017**, *8* (5), No. e01680-17.

(56) Piantini, U.; Sorensen, O. W.; Ernst, R. R. Multiple quantum filters for elucidating NMR coupling networks. *J. Am. Chem. Soc.* **1982**, *104*, 6800−6801.

(57) Rance, M.; Sørensen, O. W.; Bodenhausen, G.; Wagner, G.; Ernst, R. R.; Wüthrich, K. Improved spectral resolution in COSY (1) H NMR spectra of proteins via double quantum filtering. *Biochem. Biophys. Res. Commun.* **1983**, *117*, 479.

(58) States, D. J.; Haberkorn, R. A.; Ruben, D. J. A two-dimensional nuclear Overhauser experiment with pure absorption phase in four quadrants. *J. Magn. Reson.* **1982**, *48*, 286−292.

(59) Stern, A. S.; Li, K. B.; Hoch, J. C. Modern spectrum analysis in multidimensional NMR spectroscopy: comparison of linear-prediction extrapolation and maximum-entropy reconstruction. *J. Am. Chem. Soc.* **2002**, *124*, 1982−1993.

(60) *Schrödinger Release 2019−1*; Maestro: New York, NY, 2019.

(61) Frisch, M. J.; Trucks, G. W.; Schlegel, H. B.; Scuseria, G. E.; Robb, M. A.; Cheeseman, J. R.; Scalmani, G.; Barone, V.; Petersson, G. A.; Nakatsuji, H.; Li, X.; Caricato, M.; Marenich, A. V.; Bloino, J.; Janesko, B. G.; Gomperts, R.; Mennucci, B.; Hratchian, H. P.; Ortiz, J. V.; Izmaylov, A. F.; Sonnenberg, J. L.; Williams-Young, D.; Ding, F.; Lipparini, F.; Egidi, F.; Goings, J.; Peng, B.; Petrone, A.; Henderson, T.; Ranasinghe, D.; Zakrzewski, V. G.; Gao, J.; Rega, N.; Zheng, G.; Liang, W.; Hada, M.; Ehara, M.; Toyota, K.; Fukuda, R.; Hasegawa, J.; Ishida, M.; Nakajima, T.; Honda, Y.; Kitao, O.; Nakai, H.; Vreven, T.; Throssell, K.; Montgomery, J. A., Jr.; Peralta, J. E.; Ogliaro, F.; Bearpark, M.; Heyd, J. J.; Brothers, E. N.; Kudin, K. N.; Staroverov, V. N.; Kobayashi, R.; Normand, J.; Raghavachari, K.; Rendell, A.; Burant, J. C.; Iyengar, S. S.; Tomasi, J.; Cossi, M.; Millam, J. M.; Klene, M.; Adamo, C.; Cammi, R.; Ochterski, J. W.; Martin, R. L.; Morokuma, K.; Farkas, O.; Foresman, J. B.; Fox, D. J. *Gaussian 16*, revision B.01; Gaussian, Inc.: Wallingford CT, 2016.

(62) Case, D.; Berryman, J.; Betz, R.; Cerutti, D.; Cheatham, T., III; Darden, T.; Duke, R.; Giese, T.; Gohlke, H.; Goetz, A. *AMBER 2015*; University of California: San Francisco, 2015.

■ NOTE ADDED AFTER ASAP PUBLICATION

This paper was published ASAP on July 30, 2020. The abstract graphic and Figure 3 were updated. The revised paper was reposted on August 6, 2020.